

Chk2 sustains PLK1 activity in mitosis to ensure proper chromosome segregation

Received: 19 March 2024

Accepted: 25 November 2024

Published online: 30 December 2024



Elizabeth M. Black^{1,2}, Carlos Andrés Ramírez Parrado^{1,2}, Isabelle Trier^{1,2}, Wenxue Li^{2,3}, Yoon Ki Joo^{1,2}, Jennifer Pichurin^{1,2}, Yansheng Liu^{2,3} & Lilian Kabeche^{1,2}✉

Polo-like kinase 1 (PLK1) protects against genome instability by ensuring timely and accurate mitotic cell division, and its activity is tightly regulated throughout the cell cycle. Although the pathways that initially activate PLK1 in G2 are well-characterized, the factors that directly regulate mitotic PLK1 remain poorly understood. Here, we identify that human PLK1 activity is sustained by the DNA damage response kinase Checkpoint kinase 2 (Chk2) in mitosis. Chk2 directly phosphorylates PLK1 T210, a residue on its T-loop whose phosphorylation is essential for full PLK1 kinase activity. Loss of Chk2-dependent PLK1 activity causes increased mitotic errors, including chromosome misalignment, chromosome missegregation, and cytokinetic defects. Moreover, Chk2 deficiency increases sensitivity to PLK1 inhibitors, suggesting that Chk2 status may be an informative biomarker for PLK1 inhibitor efficacy. This work demonstrates that Chk2 sustains mitotic PLK1 activity and protects genome stability through discrete functions in interphase DNA damage repair and mitotic chromosome segregation.

Accurate mitotic progression is essential for proper cellular and organismal function, and errors in this process can both initiate and drive cancer development^{1–4}. One protein that protects against such defects is Polo-like kinase 1 (PLK1), which promotes proper centrosome maturation, bipolar spindle formation, centromere identity, kinetochore-microtubule attachment, chromosome segregation, and cytokinesis^{5–14}. Tight spatial and temporal regulation of PLK1 is necessary to accomplish these pleiotropic functions^{15–19}, and even partial reduction in PLK1 activity can lead to genome instability, senescence, and failure to proliferate^{8,20}. Thus, comprehensively identifying the factors that regulate mitotic PLK1 is important to better understand how mitotic cell division is controlled and identify pathways that protect genome stability.

PLK1 is initially activated in G2 through a highly synchronized positive feedback loop with the mitotic kinases CDK1 and Aurora A. CDK1-Cyclin A activates Aurora A by promoting its association with its activating cofactor Bora^{21–24}. Active Aurora A-Bora then activates PLK1 by directly phosphorylating T210, a residue on PLK1's T-loop whose

phosphorylation promotes PLK1 activity^{21,22,25,26}. PLK1 activity then promotes CDK1-Cyclin B activity by activating the CDK1-promoting phosphatase CDC25C and inhibiting the CDK1-inhibiting kinase Myt1^{27–29}. This positive feedback loop ensures that CDK1, Aurora A, and PLK1 are highly active as cells enter mitosis. In the presence of DNA damage, however, signaling proteins in the DNA damage response pathway inactivate CDK1 to trigger a reversible G2/M arrest^{30–32}.

Although the mechanisms that activate PLK1 in G2 are well-defined, we have an incomplete understanding of the factors that regulate PLK1 in mitosis. After mitotic entry, Bora is mostly degraded, and Aurora A associates with other co-factors, including TPX2^{22,33–35}. While there is a small residual population of Aurora A-Bora that can continue to sustain PLK1 activity in mitosis, its contribution is limited to only ~20% of PLK1 activity³⁶. PLK1 activity, however, must remain high throughout mitosis despite negative regulation from phosphatases^{37–39}. This observation suggests that there may be undescribed factors that act on PLK1 to sustain its activity in mitosis.

¹Department of Molecular Biophysics and Biochemistry, Yale University, New Haven, CT 06511, USA. ²Yale Cancer Biology Institute, Yale University, West Haven, CT 06516, USA. ³Department of Pharmacology, Yale University, New Haven, CT 06511, USA. ✉e-mail: Lilian.kabeche@yale.edu

Chk2 is an effector kinase in the DNA damage response pathway that has a well-characterized role to control cell cycle progression following DNA double-stranded breaks. In addition to this canonical role in the interphase DNA damage response, Chk2 has been implicated in a variety of mitotic processes, including checkpoint signaling, spindle formation, cytokinesis, and chromosome segregation, suggesting that Chk2 may have an important role in mitosis^{40–49}. These previous studies, however, utilized depletion methods such as knockdown or knockout that rely on natural protein turnover over multiple cell cycles, confounding the known interphase and putative mitotic functions of Chk2. These studies also lack a unifying mechanism to fully explain whether and how Chk2 could be executing these mitotic functions. Given that many of the defects associated with Chk2 deficiency mimic those observed following PLK1 inhibition^{8,50}, we hypothesized that there may be a previously unreported relationship between Chk2 and PLK1.

Here, we identify that Chk2 promotes PLK1 activity in mitosis, and that inhibiting this pathway causes chromosome segregation defects and genome instability. Our data suggest a model where this effect occurs in part through direct phosphorylation of PLK1 T210 by Chk2. We propose a paradigm whereby the mechanisms that initially activate PLK1 are distinct from those that sustain it, and that Chk2 protects genome stability through discrete functions in interphase DNA damage response and mitotic chromosome segregation.

Results

Chk2 inhibition reduces mitotic PLK1 activity

To test whether Chk2 regulates mitotic PLK1 activity, we used nocodazole to arrest cells in mitosis, isolated mitotic cells via shake off, and subsequently treated cells with inhibitors of PLK1 (1 μ M BI-2536⁵¹, PLK1i), Chk2 (10 μ M BML-277⁵², Chk2i), or a vehicle control (DMSO), and measured the abundance of phosphorylated TCTP Serine 46 (p-TCTP), a marker of PLK1 activity⁵³. We observed that treatment with Chk2i caused a ~25% decrease in p-TCTP in HeLa (cervical adenocarcinoma), RPE-1 (non-transformed retinal pigmented epithelium), PANC1 (pancreatic ductal adenocarcinoma), U2OS (osteosarcoma), and A549 (lung adenocarcinoma) cells (Fig. 1A, Supplementary Fig. 1A). p-TCTP was similarly decreased following mitotic arrest with the Eg5 inhibitor S-trityl-L-cysteine⁵⁴ (STLC, 10 μ M) and kinase inhibition (Fig. 1B). This effect is not due to degradation of PLK1 or TCTP, as inhibitor treatment did not cause changes in total protein abundance (Fig. 1A, Supplementary Fig. 1B–D). Inhibitor treatment also did not affect the abundance or foci count of γ H2AX, a marker of DNA damage (Supplementary Fig. 2A–C)⁵⁵. Taken together, these data suggest that Chk2 kinase activity is necessary to sustain full PLK1 activity in mitosis in cancerous and noncancerous cell types.

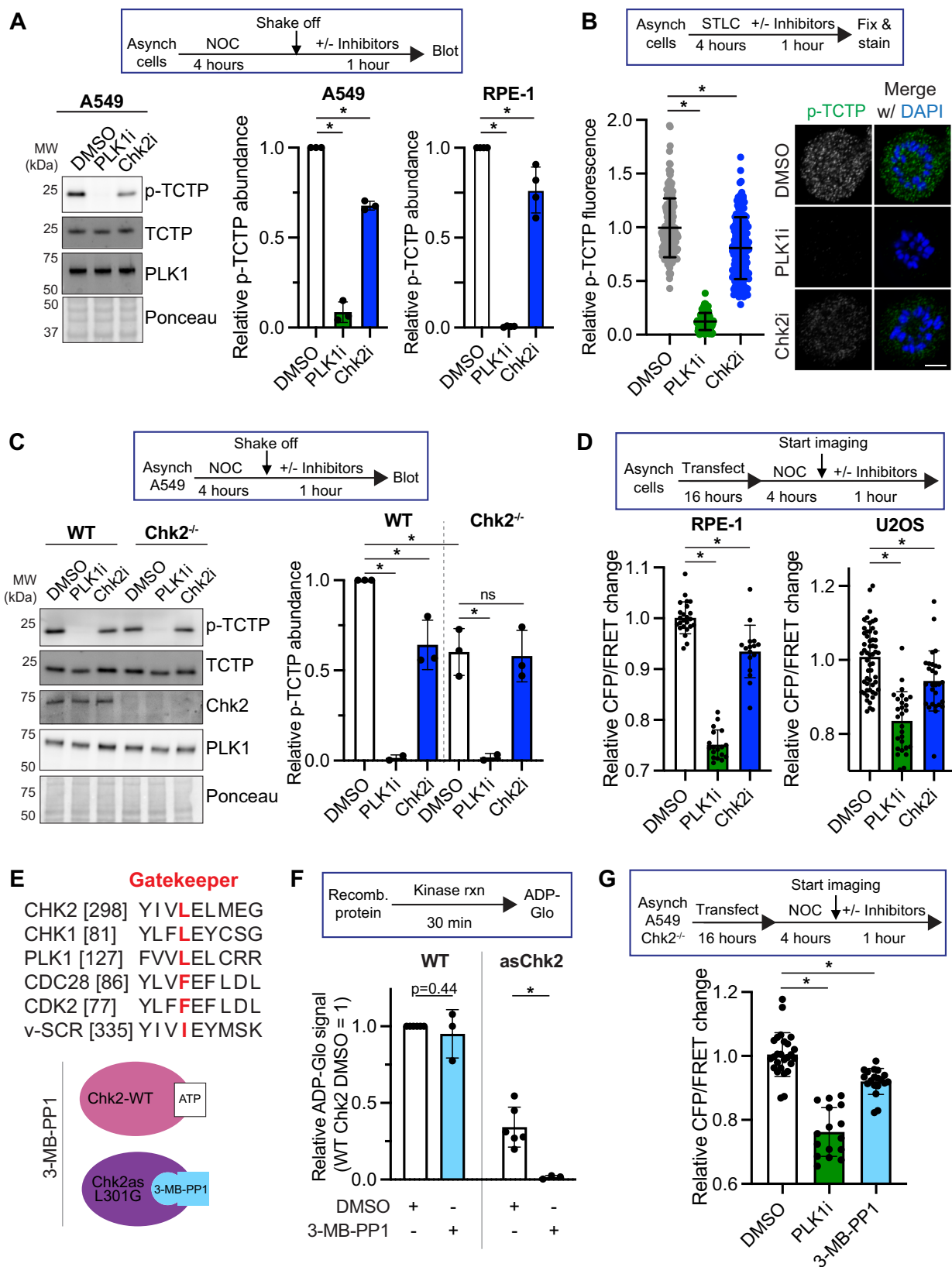
We validated that 10 μ M Chk2i abrogates Chk2 function by inducing DNA damage with doxorubicin in combination with varying concentrations of Chk2i. We measured the abundance of p53, whose stabilization following DNA damage is a canonical output for Chk2 activity⁵⁶. 10 μ M Chk2i reduced p53 accumulation compared to doxorubicin and a vehicle control, and higher doses of Chk2i did not further attenuate p53 stabilization, indicating that Chk2 is effectively inhibited at this concentration (Supplementary Fig. 2D). To validate the specificity of Chk2i, we tested whether Chk2i affects the activities of purified PLK1 and Aurora A, an important regulator of PLK1^{22,25,36}, in vitro using ADP-Glo⁵⁷. We did not observe significant inhibition of either kinase by Chk2i (Supplementary Fig. 3A). Furthermore, we compared PLK1 activity in Chk2-proficient (wild-type, WT) and -deficient (Chk2^{-/-}, Supplementary Fig. 3B) A549 cells treated with a vehicle control, PLK1i, or Chk2i. Chk2^{-/-} cells have ~30% less p-TCTP compared to WT cells, comparable to Chk2i-treated WT cells (Fig. 1C, Supplementary Fig. 3C) without affecting total levels of TCTP (Supplementary Fig. 3D). Chk2i treatment did not further affect p-TCTP in Chk2^{-/-} cells, providing evidence for the specificity of the inhibitor in this

context. We also observed reduced p-TCTP in nocodazole-arrested HeLa cells treated with a Chk2-targeting siRNA compared to a non-targeting siRNA (Supplementary Fig. 3E). Similarly, we found that treating A549 and HeLa cells with a structurally distinct⁵⁸ (3.4 μ M), caused a ~30% reduction in p-TCTP without affecting total TCTP levels (Supplementary Fig. 4A, B). Chk2i also does not inhibit PLK1 in vitro (Supplementary Fig. 4C). Together, these data demonstrate that independent genetic and chemical approaches to disrupt Chk2 activity also lead to reduced mitotic PLK1 activity.

We used a chemical genetics approach to validate that p-TCTP is a reliable readout for PLK1 activity. Analog-sensitive (as) alleles contain mutations to the kinase ATP binding pocket that increase the size of the binding pocket, rendering the protein uniquely susceptible to inhibition with 3-MB-PP1, a bulky and nonhydrolyzable ATP analog. When we add 3-MB-PP1 to RPE-1 cells expressing asPLK1-GFP⁶, we observed a complete loss of p-TCTP signal, demonstrating that p-TCTP S46 is a specific output for PLK1 activity (Supplementary Fig. 4D). As an additional readout of PLK1 activity, we used an engineered FRET sensor whose conformation and subsequent FRET emission is correlated with PLK1 activity⁷ (Supplementary Fig. 4E). One-hour PLK1i treatment of nocodazole-arrested U2OS and RPE-1 cells led to a ~20–25% decrease in normalized CFP/FRET signal (Fig. 1D, Supplementary Fig. 4F). In comparison, Chk2i treatment led to a ~7% decrease in normalized CFP/FRET signal (Fig. 1D). These data support our observation that Chk2 inhibition leads to a partial reduction in mitotic PLK1 activity.

To get a more global understanding of how Chk2 affects PLK1 activity, we performed a kinase reaction on lysates from mitotic asPLK1-GFP cells in the presence of a bulky labeled ATP analog (N6-Benzyl-ATP- γ S) to selectively visualize PLK1 kinase activity. Because asPLK1 has a mutation to the gatekeeper residue that allows the protein to utilize bulky ATP analogs that would otherwise be sterically hindered, we can visualize PLK1-specific substrates by reacting the γ -thiophosphate of N6-Benzyl-ATP- γ S with p-nitrobenzyl mesylate (PNBM, 2.5 mM), an alkylating agent, to generate a thiophosphate ester (TPE) epitope. Signal from the TPE antibody, therefore, indicates specific and direct substrates of asPLK1 (Supplementary Fig. 5A). We performed this reaction in the presence of 3-MB-PP1, which will inhibit asPLK1 and serve as a negative control, Chk2i, or DMSO. There was reduced TPE signal in the Chk2i-treated reaction compared to the DMSO-treated reaction, and this signal reduction appears largely homogenous across all substrates, further supporting that Chk2 affects global PLK1 activity (Supplementary Fig. 5B).

Finally, we sought to develop a chemical genetics approach to validate that Chk2 sustains PLK1 activity. We engineered an asChk2 allele by mutating Chk2's gatekeeper residue, a conserved amino acid in the ATP binding pocket, from Leucine to Glycine. This mutation increases the size of the ATP-binding pocket and renders the protein susceptible to inhibition with 3-MB-PP1 (Fig. 1E). We purified WT and asChk2 (L301G) from *E. coli* (Supplementary Fig. 5C, D) and determined their relative activities in the presence of DMSO or 3-MB-PP1 using ADP-Glo (Supplementary Fig. 5E). Although asChk2 had lower basal activity than WT Chk2, we observed that only asChk2 activity was significantly affected by treatment with 3-MB-PP1 (Fig. 1F), demonstrating the selectivity of this inhibitor for the as-kinase and our ability to use asChk2 as a genetic tool to study Chk2 function. We measured PLK1 activity in Chk2^{-/-} A549 cells that were transiently co-transfected with the PLK1 FRET sensor and mCherry-asChk2. Cells expressing asChk2 treated with 3-MB-PP1 demonstrated a significant decrease in the CFP/FRET ratio (Fig. 1G), reflecting a decrease in PLK1 activity. In contrast, cells that did not express asChk2 (mCherry-negative) had no significant change in the CFP/FRET ratio following 3-MB-PP1 treatment (Supplementary Fig. 5F), indicating that this effect is specific to inhibiting asChk2. These data use a chemical genetics approach to further support our observation that Chk2 sustains PLK1 activity in mitosis.



Chk2 activity towards PLK1 is independent of the DNA damage response pathway. We wanted to identify whether this function for Chk2 in regulating mitotic PLK1 activity is dependent on ATM, a well-characterized Chk2 activator in response to DNA damage^{32,59,60}. First, we validated that U2OS and HeLa cells are ATM-proficient by treating cells with doxorubicin to induce DNA damage and ATM signaling. We

observed increased phosphorylation of the canonical ATM substrate p-Chk2 S33/35⁶¹ following doxorubicin treatment, and this increase was sensitive to treatment with ATM inhibitor (ATMi, 10 μ M KU55933⁶², Supplementary Fig. 6A). ATMi in mitotic U2OS cells, however, did not significantly affect PLK1 activity as measured by CFP/FRET emission for the PLK1 FRET sensor or p-TCTP abundance (Fig. 2A,

Fig. 1 | Chk2 sustains mitotic PLK1 activity. **A** Top, experimental setup. Following 4-h treatment with 100 ng/mL nocodazole (NOC), mitotic cells were collected via shake off and treated for 1 h with PLK1i (1 μ M BI-2536), Chk2i (10 μ M BML-277), or DMSO, then collected and immunoblotted. Left, representative blot of A549 cells. Right, quantification of $N = 3$ (A549) or $N = 4$ (RPE-1) biological replicates. $*p < 0.05$, two-tailed t -test. **B** Following 4-hour arrest in 10 μ M S-trityl-L-cysteine (STLC), inhibitors or DMSO were added for 1 h. Cells were then fixed and stained for p-TCTP. Scale bar, 5 μ m. Points are individual cells ($n = 172$ DMSO, 115 PLK1i, 168, Chk2i) combined from 3 experiments. $*p < 0.05$, two-tailed t -test of normalized replicate means. **C** A549 wild-type (WT) or Chk2^{-/-} cells treated as in (A). Right, quantification of $N = 3$ (DMSO, Chk2i) or $N = 2$ (PLK1i) experimental replicates. $*p < 0.05$, unpaired one-way ANOVA with Bonferroni multiple comparison correction. ns, not significant. **D** Quantification of normalized CFP/FRET change for each condition in RPE-1 and U2OS cells. Error bars SD of individual cell values combined from $N = 3$ (U2OS) or $N = 5$ (RPE-1) experimental replicates. Individual cells $n = 24$,

RPE-1 DMSO; $n = 18$, RPE-1 PLK1i; $n = 16$, RPE-1 Chk2i; $n = 56$, U2OS DMSO; $n = 28$ U2OS PLK1i; $n = 28$ U2OS Chk2i. $*p < 0.05$, two-tailed t -test of individual cell values. DMSO values are the same as in Fig. 2A. **E** Top, protein sequence alignment of kinase ATP-binding pocket residues. Putative gatekeeper residues are red. Bottom, cartoon of analog-sensitive (as)Chk2 allele. **F** ADP-Glo quantification of kinase activity with DMSO or 10 μ M 3-MB-PP1. Points denote an experimental replicate. Error bars SD ($N = 6$ WT and asChk2 DMSO; $N = 3$ WT and asChk2 3-MB-PP1). ns not significant, $*p < 0.05$, two-tailed t -test. **G** Quantification of relative change in CFP/FRET ratio 1 h after addition of inhibitors or DMSO in cells co-expressing PLK1 FRET and asChk2-mCherry. Each point represents one cell normalized to the average value in the DMSO condition for each replicate. Error bars SD of individual cell values combined from ≥ 3 experimental replicates, $n = 26$ DMSO, $n = 16$ PLK1i, $n = 19$ Chk2i. $*p < 0.05$, two-tailed t -test of individual cell values. All panels, data are presented as mean values \pm SD. Source data are provided as a Source Data file.

Supplementary Fig. 6B), suggesting that ATM may not be acting upstream of Chk2 in mitosis.

Although ATM is the best-characterized Chk2 activator, other apical DNA damage response kinases, including ATR and DNA-PK, have also been reported to activate Chk2^{63,64}. To test whether these kinases affect PLK1 activity, we treated isolated nocodazole-arrested HeLa cells with small molecule inhibitors of ATM, DNA-PK (DNA-PKi, 5 μ M M3814⁶⁵), and ATR (ATRi, 10 μ M AZ20⁶⁶). We did not observe any significant change in p-TCTP or TCTP with these inhibitors compared to a DMSO control (Fig. 2B, Supplementary Fig. 6C). In contrast, inhibitor treatment led to reduced phosphorylation of the ATM and DNA-PK substrate γ H2AX and the ATR substrate phospho-Chk1 S317, demonstrating inhibitor efficacy (Fig. 2B). Together, these data demonstrate that ATM, DNA-PK, and ATR do not affect PLK1 activity in mitosis and suggest that mitotic Chk2 activity is independent of canonical upstream regulators in the DNA damage response pathway.

We confirmed a recent report that the nonreceptor tyrosine kinase Janus kinase 2 (JAK2) promotes mitotic Chk2 activity⁴⁵ and found that JAK2 inhibition (JAK2i, 5 μ M JAK2 inhibitor IV⁶⁷) also reduces PLK1 activity in nocodazole-arrested U2OS and HeLa cells by ~30%, comparable to the reduction we observed following treatment with Chk2i (Fig. 2C, Supplementary Fig. 6E). Total TCTP levels, in contrast, were not affected (Supplementary Figs. 6D, S6F). Combinatorial treatment of JAK2i and Chk2i did not decrease p-TCTP beyond either inhibitor alone (Fig. 2C, Supplementary Fig. 6E), suggesting that JAK2 and Chk2 work in the same pathway to promote PLK1 activity. This is not due to off-target effects of JAK2i on Chk2 or PLK1 (Supplementary Fig. 6G). To further validate whether JAK2's effect on PLK1 is dependent on Chk2, we treated nocodazole-arrested A549 WT and Chk2^{-/-} cells with JAK2i and observed that JAK2i did not further decrease p-TCTP or TCTP levels in Chk2^{-/-} cells (Fig. 2D, Supplementary Fig. 6H), supporting the hypothesis that noncanonical activation of Chk2 by JAK2 is important for regulating mitotic PLK1 activity.

Chk2 directly phosphorylates PLK1 T210

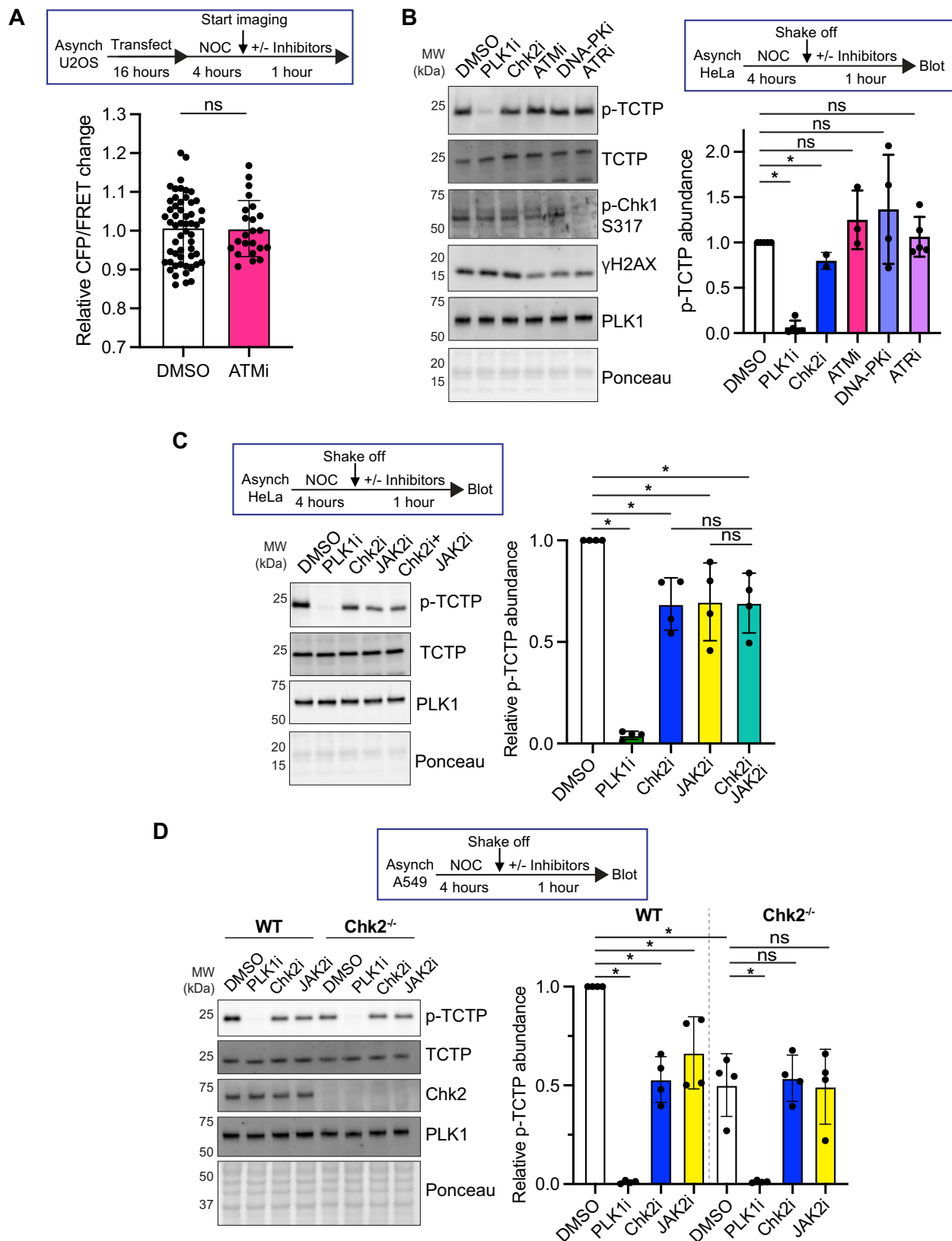
To identify potential mechanisms by which Chk2 promotes PLK1 activity, we sought to determine if Chk2 modulates the known PLK1-regulatory kinases CDK1 and Aurora A. CDK1 primes PLK1 activity by phosphorylating key scaffolding proteins at the centrosome, centromere, and kinetochore, which in turn recruit PLK1 through its polo-binding domains^{15,18,68,69}. One-hour treatment of mitotic U2OS cells treated with the proteasome inhibitor MG132 (20 μ M) and CDK1 inhibitor (CDK1i, 5 μ M RO-3306⁷⁰) led to a significant reduction in PLK1 activity, measured by p-TCTP (Fig. 3A). Combinatorial treatment with CDK1i and Chk2i in the presence of MG132 further reduced p-TCTP, suggesting that Chk2 works independently of CDK1 to promote PLK1 activity (Fig. 3A). These changes are not due to reduced TCTP levels (Supplementary Fig. 7A) or premature mitotic exit following treatment with CDK1i, as cyclin B levels were unaffected (Fig. 3A). Furthermore,

Chk2i does not affect the abundance of phospho-PRC1 T481 (p-PRC1), a known mitotic CDK1 substrate⁷¹ (Supplementary Fig. 7B, C). These data are consistent with our model that Chk2 promotes PLK1 activity independently of CDK1.

Aurora A, alongside its cofactor Bora, activates PLK1 in G2 by phosphorylating PLK1 T210, a residue in PLK1's T-loop essential for robust PLK1 activity^{22,25,26}. Bora is mostly degraded at mitotic entry, and Aurora A's contribution to sustaining PLK1 activity in mitosis is limited to ~15–20%^{35,36}. Consistent with prior reports³⁶, acute Aurora A inhibition (AurAi, 50 nM MLN8237⁷²) of mitotic U2OS cells led to a ~15% loss of p-TCTP without affecting total TCTP levels (Fig. 3B, Supplementary Fig. 7D). Co-treatment of mitotic cells with AurAi and Chk2i did not further decrease p-TCTP beyond Chk2i, indicating that Aurora A activity may contribute to some of the reduction in PLK1 activity following treatment with Chk2i. However, the total decrease in p-TCTP with Chk2i was greater than AurAi alone, indicating that changes in Aurora A activity are not sufficient to fully explain the change in PLK1 activity we observe with Chk2i. In support of this model, we did not observe significant changes in the abundance of phospho-Aurora A T288 (p-AurA), a marker of active Aurora A, in Chk2i-treated cells when we blotted with an antibody that recognizes phosphorylated Aurora A/B/C kinases, suggesting that Chk2 is not exclusively working through Aurora A to regulate PLK1 (Fig. 3B, Supplementary Fig. 7E). Taken together, these data demonstrate that Chk2 does not sustain mitotic PLK1 activity exclusively by modulating the known PLK1 regulators CDK1 and Aurora A.

Because PLK1 activity is regulated through phosphorylation^{25,26,36,73–76}, we tested the hypothesis that PLK1 phosphorylation is affected following acute treatment with Chk2i. We detected phosphorylated PLK1 with a PhosTag gel, where the migration of phosphorylated proteins is slowed, resulting in apparently higher molecular weight species that are not present in a SDS-PAGE gel and are sensitive to treatment with exogenous protein phosphatases (Supplementary Fig. 7F)⁷⁷. We observed a ~25% reduction in the proportion of phosphorylated PLK1 in mitotic HeLa cells treated with Chk2i compared to DMSO (Fig. 3C), suggesting that Chk2 promotes PLK1 phosphorylation in mitosis.

One of the most important and well-studied regulatory phosphorylation sites on PLK1 is T210, whose phosphorylation is both necessary and sufficient to promote PLK1 activity^{25,26,36,73}. Using antibodies that are specific to PLK1 T210 phosphorylation (p-T210, Supplementary Figs. 7F, 8A), we confirmed that p-T210 is sensitive to treatment with Aurora A inhibitor, as Aurora A is the canonical kinase that phosphorylates this substrate (Supplementary Fig. 8B). We next tested whether PLK1 T210 phosphorylation is reduced in mitotic cells following Chk2i treatment by immunoprecipitating PLK1 from mitotic U2OS cells and measuring p-T210. Treatment with Chk2i significantly (~25%) reduced p-T210 normalized to the total immunoprecipitated PLK1 (Fig. 3D, E), and this effect was reproducible with two



independent antibodies (Cell Signaling Technology #5472 and #D5H7). Likewise, we probed the immunoprecipitated protein with an antibody that recognizes phosphorylated Serine or Threonine residues with an Arginine at the -3 position (R-X-X-pS/pT), as PLK1 T210 matches this motif (R-K-K-T₂₁₀). We observed that Chk2-treated cells had a similar decrease in signal from the phospho-antibody (Fig. 3D, E),

consistent with the observation that this phosphorylation site is sensitive to treatment with Chk2i.

Chk2's consensus substrate motif is highly basophilic, raising the possibility that PLK1 T210, which has basic residues in at the -1, -2, and -3 positions, may be a favorable Chk2 substrate^{78,79}. PLK1 T210 scores above the 97th percentile as a computationally predicted

Fig. 2 | Chk2 works in concert with JAK2 to promote PLK1 activity.

A Quantification of relative change in CFP/FRET ratio 1 h after addition of ATMi (10 μ M KU55933) or DMSO in 100 ng/mL nocodazole-arrested U2OS cells. DMSO values are the same as in Fig. 1D. Each point denotes one cell. Values are combined from ≥ 3 experimental replicates. $n = 56$ cells for DMSO, $n = 23$ cells for ATMi. ns, not significant ($p > 0.05$), two-tailed t -test. Error bars SD of individual cell values. **B** Top, experimental setup. Following 4-h treatment with nocodazole (NOC, 100 ng/mL), mitotic cells were collected via shake off and centrifugation. These mitotic cells were then resuspended in a smaller volume of the original media and treated for 1 h with PLK1i (1 μ M BI-2536), Chk2i (10 μ M BML-277), ATMi (10 μ M KU55933), DNA-PKi (5 μ M M3814), ATRi (10 μ M AZ-20), or equal volume DMSO. Following inhibitor treatment, cells were collected and immunoblotted. Right, quantification of ≥ 3 experimental replicates. Each point demarcates value from biological replicate. $N = 5$ DMSO, $N = 5$ PLK1i, $N = 2$ Chk2i, $N = 3$ ATMi, $N = 4$ DNA-PKi, $N = 5$ ATRi. Error

bars SD. $*p < 0.05$, two-tailed t -test. ns, not significant. **C** Top, experimental setup. Isolated mitotic HeLa cells were treated for 1 h with PLK1i (1 μ M BI-2536), Chk2i (10 μ M BML-277), JAK2i (5 μ M JAK2 inhibitor IV), combination of Chk2i and JAK2i, or equal volume DMSO as a vehicle control. Following inhibitor treatment, cells were collected and immunoblotted. Left, representative western blot. Right, quantification of 4 experimental replicates. Each point demarcates the value from one experimental replicate. Error bars SD. $*p < 0.05$, one-way Anova with Bonferroni multiple comparison correction. **D** Top, experimental setup. Isolated mitotic A549 WT and Chk2^{-/-} cells were treated as in 2C. Left, representative western blot. Right, quantification of 4 experimental replicates. Each point demarcates value from biological replicate. Error bars SD. $*p < 0.05$, one-way anova with Bonferroni multiple comparison correction. All panels, data are presented as mean values \pm SD. Source data are provided as a Source Data file.

Chk2 substrate (that is, PLK1 T210 scores more favorably as a Chk2 substrate than 97% of putative phosphorylation sites in the phosphoproteome)⁷⁸. This prompted our hypothesis that Chk2 may directly phosphorylate PLK1 T210 to sustain its activity in mitosis. We sought to determine whether Chk2 can directly phosphorylate PLK1 by performing an in vitro kinase assay where we co-incubated catalytically active MBP-Chk2 and HIS-PLK1. We observed that co-incubated Chk2 and PLK1 had increased R-X-X-pS/pT and p-T210 signal at PLK1's molecular weight compared to PLK1 alone (Fig. 3F). This signal was sensitive to treatment with Chk2i, but not PLK1i, suggesting that this is due to direct phosphorylation of PLK1 by Chk2, rather than PLK1 autophosphorylation. We performed a similar kinase reaction with active or kinase-dead (KD) Chk2 in which T383 and T387 are mutated to Alanine to abrogate activity⁸⁰. Similarly, only the active form of Chk2 was able to phosphorylate PLK1 (Supplementary Fig. 8C). To test whether this effect is specific to Chk2, we co-incubated recombinant catalytically active CDK1-Cyclin B-HIS or Chk2-MBP with PLK1. Chk2, but not CDK1-Cyclin B, was able to robustly phosphorylate PLK1 T210 (Supplementary Fig. 8D). Finally, we used Parallel Reaction Monitoring (PRM)-based mass spectrometry to measure the abundance of phospho-PLK1 T210 following co-incubation of active GST-Chk2 and HIS-PLK1 in the presence of DMSO or Chk2i, as in Fig. 3F. Using a synthetic heavy-labelled standard peptide, we verified the existence of phospho-PLK1 T210 in the kinase reaction and calculated that this phospho-peptide was 1.8 times more abundant in the DMSO-treated reaction than in the reaction with Chk2i (Supplementary Fig. 8E), supporting the idea that PLK1 T210 is a Chk2 substrate. We next sought to determine the dynamics of PLK1 T210 turnover in mitosis. We inhibited PP-2A, the phosphatase that removes T210 phosphorylation, by treating cells with 100 nM okadaic acid and found that PLK1 T210 phosphorylation increases by ~25%, consistent with prior reports (Supplementary Fig. 8F)³⁹. These data indicate that T210 phosphorylation turns over during mitosis, and that this phosphorylation, and by extension PLK1 activity, requires active input from other kinases to sustain its activity. Together, these data support a model in which Chk2 directly phosphorylates PLK1 T210 to sustain PLK1 activity in mitosis.

PLK1 and Chk2 activity promote proper mitotic progression

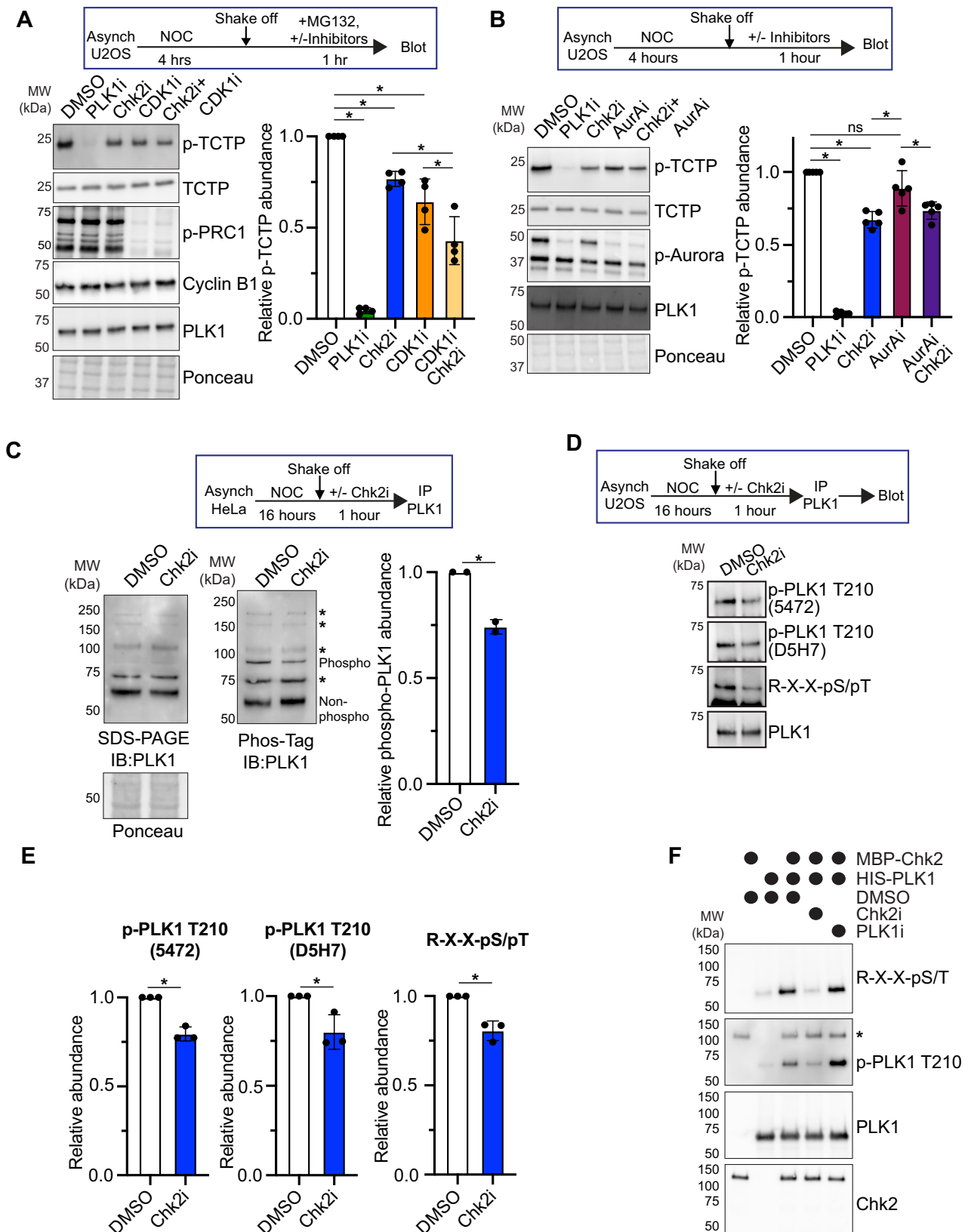
PLK1 promotes proper mitotic progression through its roles in centrosome maturation, bipolar spindle formation, kinetochore-microtubule attachment, chromosome segregation, and cytokinesis^{5–13}. We hypothesized that the partial reduction in PLK1 activity following Chk2i may induce defects in some of these processes, as previous work has identified that these PLK1 functions are differentially sensitive to partial inhibition⁸. To tease apart the PLK1-dependent and -independent effects of mitotic Chk2 inhibition, we identified a dose of PLK1i (5 nM) that simulates the ~30% reduction in p-TCTP that we observe following Chk2i in nocodazole-arrested RPE-1 cells (Supplementary Fig. 9A). 5 nM PLK1i also caused a similar decrease in nocodazole-arrested U2OS cells (Supplementary Fig. 9B) and in asynchronous prometaphase and metaphase

RPE-1 cells (Fig. 4A, B) without affecting total TCTP levels (Supplementary Fig. 9B–D).

PLK1 localizes to, and is active at, the centrosome and kinetochore, and its localization is partially dependent on its kinase activity^{16,81}. We treated asynchronous RPE-1 cells with 5 nM PLK1i, Chk2i, or DMSO for 1 h and measured PLK1 localization to centrosomes, marked by pericentrin, and kinetochores, marked by anti-centromere antibody (ACA). Importantly, this experimental setup with acute, 1-hour inhibitor treatment provides high temporal resolution to differentiate the mitotic and interphase effects of perturbing kinase signaling. Cells treated with 5 nM PLK1i or Chk2i had reduced PLK1 localization to kinetochores and centrosomes in both prometaphase and metaphase (Supplementary Fig. 10A, B), suggesting that Chk2 is important for promoting proper localization and activity for multiple populations of PLK1. To gain further insight into the spatial regulation of PLK1, we sought to determine Chk2 localization in mitotic cells. We expressed a FLAG-tagged Chk2 construct in HCT-116 cells and observed diffuse cytoplasmic localization with an enrichment on the spindle in prometaphase and metaphase (Supplementary Fig. 10C), as previously reported^{82,83}. This localization pattern suggests that Chk2 may be in a position to directly phosphorylate and activate PLK1 throughout early mitosis.

We sought to identify the effects of acute Chk2 inhibition and partial PLK1 inhibition on proper mitotic progression. PLK1 promotes proper chromosome alignment in metaphase by phosphorylating proteins at the centromere and kinetochore that regulate the attachment to spindle microtubules and protect chromatin against microtubule pulling forces^{7,11,18}. We observed that RPE-1 and U2OS cells treated for 1 h with Chk2i or 5 nM PLK1i had significant defects in metaphase chromosome alignment (Fig. 4C), a prerequisite for accurate chromosome in anaphase⁸⁴. We observed a similar increase in metaphase misalignment in asynchronous Chk2^{-/-}, compared to WT, A549 cells (Supplementary Fig. 11A). Consistent with our model in which JAK2 acts as an upstream regulator of Chk2 in mitosis, treatment of WT, but not Chk2^{-/-}, A549 cells with JAK2i also led to an increase in metaphase chromosome misalignment compared to DMSO (Supplementary Fig. 11A).

An increased rate of anaphase chromosome missegregation is a hallmark of many kinds of cancers and is correlated with poor patient prognosis^{1–4}. We tested whether partial reduction in PLK1 activity through Chk2i or 5 nM PLK1i would affect chromosome segregation fidelity. RPE-1 and U2OS cells acutely treated with Chk2i or 5 nM PLK1i had increased rates of whole-chromosome missegregation, or lagging chromosomes, compared to vehicle-treated cells (Fig. 4E, Supplementary Fig. 11B). In contrast, inhibitor treatment did not increase the rates of acentric chromatin or chromatin bridges, which are caused by unrepaired DNA double-stranded breaks or under-replicated DNA, respectively (Fig. 4E, Supplementary Fig. 11B). We also observed that Chk2^{-/-} cells had significantly more lagging chromosomes compared to WT cells (Supplementary Fig. 11C). Acute treatment with JAK2i



phenocopied this effect in WT cells and did not further increase the rate of lagging chromosomes in Chk2^{-/-} cells (Supplementary Fig. 11C). To complement our immunofluorescence data, we performed a low-throughput live-cell imaging experiment with asynchronous H2B-GFP-expressing HeLa cells. We identified prophase cells based on chromatin compaction, added 5 nM PLK1i, Chk2i, or JAK2i to the media, and

captured their progression through mitosis. Drug addition caused a ~2–3-fold increase in the rate of chromosome missegregation compared to DMSO-treated cells (Supplementary Fig. 11D, E). Micronuclei are chromatin-containing structures distinct from the main nucleus that are formed from missegregated chromosomes. Increased numbers of micronuclei are a hallmark and driver of cancer, as they can

Fig. 3 | Chk2 regulates PLK1 through direct phosphorylation. **A** Representative western blot (left) and quantification (right) of U2OS cells treated with MG132 (20 μ M) in combination with PLK1i (1 μ M BI2536), Chk2i (10 μ M BML-277), CDK1i (5 μ M RO-3306), CDK1i Chk2i combination, or a DMSO vehicle control. Each point represents one experimental replicate * $p < 0.05$, paired 1-way ANOVA with Bonferroni multiple comparisons correction. ns not significant ($p > 0.05$). Error bars SD. **B** Representative western blot (left) and quantification (right) of U2OS cells treated with PLK1i (1 μ M BI2536), Chk2i (10 μ M BML-277), AurAi (50 nM MLN-8237), AurAi Chk2i combination, or a DMSO vehicle control. * $p < 0.05$, one-way ANOVA with Bonferroni multiple comparisons correction. ns, not significant ($p > 0.05$). Error bars SD. **C** Left, immunoblot of mitotic HeLa cells treated with a vehicle control or Chk2 inhibitor for 1 h. Right, immunoblot of the same samples on a PhosTag gel. The putative phosphorylated species of PLK1 is indicated. *, uncharacterized bands recognized by PLK1 antibody. Right, quantification of phosphorylated PLK1 (slower-migrating PLK1 band on PhosTag gel) normalized to the total PLK1 protein

abundance (68 kDa band on SDS-Page gel). Each point represents one biological replicate. * $p < 0.05$, two-tailed t -test. Error bars SD. **D** Experimental setup and representative western blot of PLK1 immunoprecipitated from mitotic HeLa cells treated with DMSO or Chk2i. **E** Quantification of phospho-antibody signal normalized to total PLK1 abundance from (D). Each point represents the value from one experimental replicate. * $p < 0.05$, two-tailed t -test. Error bars SD. **F** In vitro kinase assay with recombinant HIS-PLK1, MBP-Chk2 incubated with DMSO, PLK1i, or Chk2i as marked. Recombinant proteins were incubated in kinase assay buffer in a 1:1 molar ratio with 500 μ M ATP for 30 minutes at 30 $^{\circ}$ C with gentle agitation. The reaction was quenched with 5 mM EDTA before being combined with denaturing sample buffer and analyzed via western blotting. p-PLK1 T210 antibody shown is Cell Signaling Technology D5H7. *, nonspecific recognition of MBP-Chk2. This experiment has been replicated 5 times with similar results. All panels, data are presented as mean values \pm SD. Source data are provided as a Source Data file.

deleteriously affect gene expression, DNA damage repair, and inflammation^{2,85–89}. We measured the rate of micronuclei formation from cells that were isolated after nocodazole arrest and allowed to progress through mitosis in the presence of DMSO, Chk2i, or 5 nM PLK1i. Chk2i-treated cells had increased rates of micronuclei compared to DMSO (Supplementary Fig. 11F). Together, these data demonstrate that mitotic Chk2 activity is essential to promote proper chromosome segregation and protect genome stability through PLK1.

PLK1 activity is also important for cytokinesis at the conclusion of mitosis^{6,8}, and failure to properly complete cytokinesis can result in tetraploidy. We sought to determine if cytokinesis is also sensitive to Chk2 and partial PLK1 inhibition. Asynchronous RPE-1 cells treated with either Chk2i or 5 mM PLK1i exhibited a decreased percentage of telophase cells with a cytokinetic furrow, measured by constriction of α -tubulin between the dividing chromatin (Fig. 3F). To further illustrate the importance of this pathway for proper cytokinesis, we performed a live-cell imaging experiment with H2B-GFP-expressing HeLa cells. We arrested cells using CENP-E inhibitor (CENP-Ei, 2 μ M GSK923295⁹⁰), which induces a pseudo-metaphase arrest due to the presence of misaligned chromosomes, then added 5 nM PLK1i, Chk2i, or a DMSO control, and triggered anaphase onset by addition of MPS1 inhibitor (MPS1i, 1 μ M Reversine⁹¹) (Supplementary Fig. 11G). We then measured the time from anaphase onset to observable constriction of the cytokinetic furrow and found that cells treated with Chk2i or 5 nM PLK1i had significantly longer time to form a cytokinetic furrow than DMSO-treated cells (Supplementary Fig. 11G). These data suggest that Chk2 activity is crucial for proper PLK1 function in distinct contexts, and that even modest reductions in PLK1 activity may be deleterious to genome stability and mitotic progression. This work also highlights that some of the mitotic defects previously observed following Chk2 perturbation^{40–48} may be due to a bona fide mitotic function rather than the result of unresolved DNA damage in interphase.

Chk2 deficiency sensitizes cells to treatment with low-dose PLK1 inhibitors

PLK1 activity is essential for timely mitotic division, making it an attractive therapeutic target in cancer therapies. However, PLK1 inhibitors have thus far been unsuccessful as a clinical monotherapy, in part because of on-target toxicity⁹². We hypothesized that Chk2 deficiency, which we have shown reduces mitotic PLK1 activity, could increase cellular sensitivity to low-dose PLK1 inhibitors. We treated WT and Chk2^{-/-} A549 cells for 3 days with a titration of PLK1i and measured cell viability with crystal violet. Chk2^{-/-} cells were more sensitive to PLK1i compared to WT cells at several concentrations, most prominently around 5–10 nM (Fig. 5A). Consistent with these data, knocking down Chk2 with a siRNA (Fig. 5B) significantly increased sensitivity to low-dose (2.27 nM) PLK1i compared to a non-targeting siRNA control (Fig. 5C, Supplementary Fig. 12A–C). This observation is further supported by a recent study where Chk2 knockout was identified in an

unbiased genome-wide screen to confer vulnerability to low-dose PLK1 inhibition²⁰.

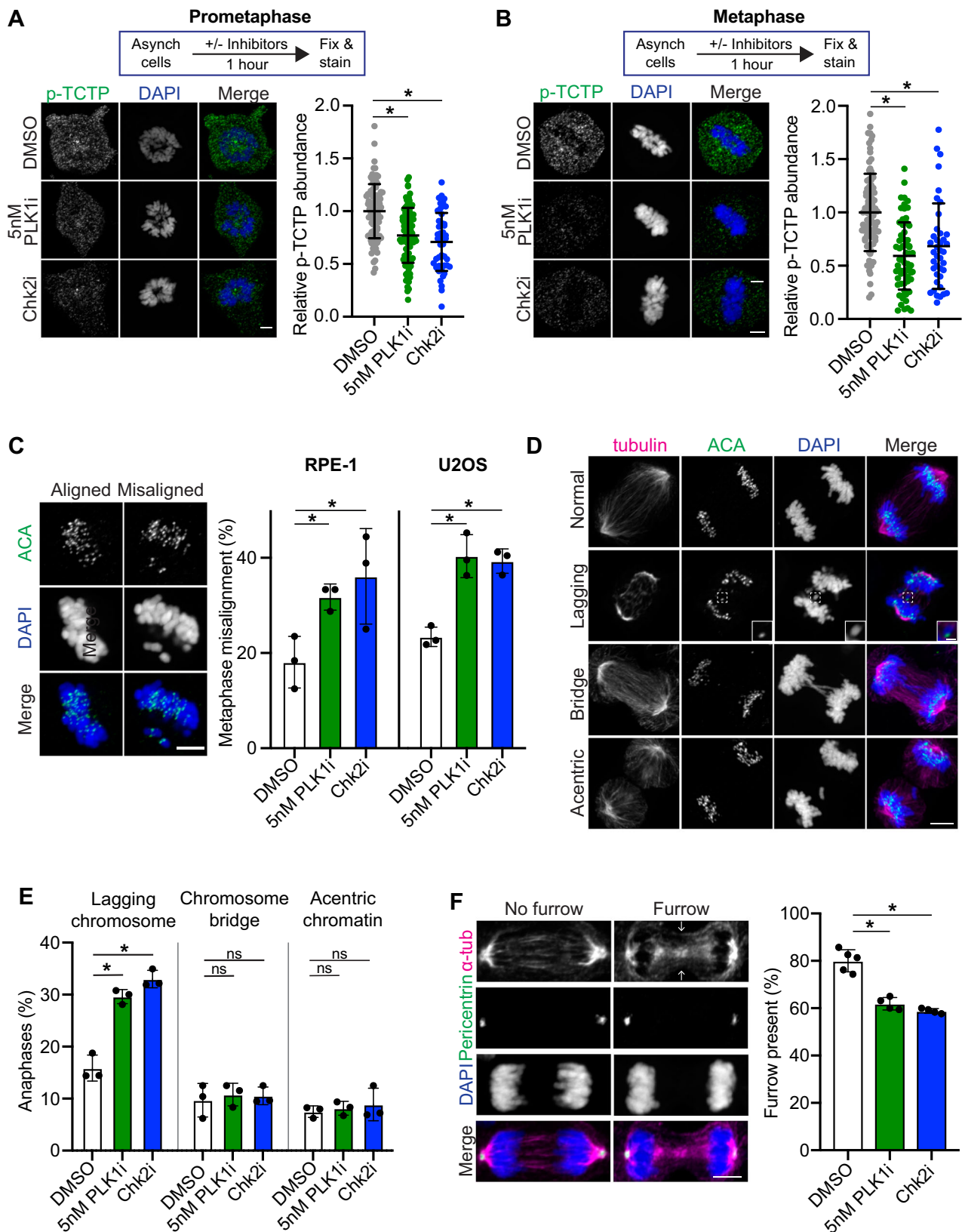
Finally, we wanted to test whether we could rescue PLK1 inhibitor sensitivity in cells carrying an endogenous Chk2 mutation. HCT-116 cells have a heterozygous L355P mutation in Chk2's kinase domain that is predicted to damage Chk2 kinase activity⁹³ (Fig. 5D). To test Chk2's functional status in HCT-116 parental cells and cells expressing an mCherry-tagged rescue construct, we induced DNA damage with the topoisomerase II inhibitor etoposide for 6 h and measured CDK1 Y15 phosphorylation (p-Y15), a canonical output of Chk2 activity⁹³. While parental HCT-116 cells had increased p-Y15 signal following DNA damage, likely because of compensation or redundancy with the DNA damage response kinase Chk1^{30,94}, they were insensitive to treatment with Chk2i (Fig. 5E). In contrast, p-Y15 abundance was sensitive to treatment with Chk2i in the rescue cell line, confirming the functional status of the Chk2 rescue line.

We measured PLK1 activity in HCT-116 cells in cells transduced with a doxycycline (DOX)-inducible 3xFLAG-Chk2 construct. Following 2 days of DOX induction, cells expressing Chk2 had significantly higher p-TCTP levels (Fig. 5F, Supplementary Fig. 12D), while total TCTP levels did not significantly change (Supplementary Fig. 12E), demonstrating that Chk2 functional status modulates PLK1 activity, and that this mitotic Chk2-PLK1 pathway may contribute to PLK1 inhibitor sensitivity. When we treated parental HCT-116 and Chk2 rescue cells with PLK1i and measured viability, we observed that Chk2-expressing cells were less sensitive to low-dose PLK1 inhibition (Fig. 5G). Together, these data demonstrate that Chk2 status may be a predictive biomarker of PLK1i sensitivity, and that Chk2 deficiency could be a therapeutic niche in which PLK1 inhibitors are an effective cancer therapeutic strategy.

Discussion

PLK1 is a well-established safeguard of the genome in part through its multiple mitotic functions. Tight control of PLK1's spatiotemporal localization, as well as its precise activity, is essential for proper chromosome segregation. Chk2 protects genome stability through its role in the DNA damage response pathway, where it counteracts CDK1 and PLK1 activity as part of the G2/M checkpoint. Our data reveal an unexpected function for Chk2 to sustain PLK1 activity in mitosis. Disruptions to this pathway lead to mitotic errors, including impaired chromosome alignment, chromosome segregation, and cytokinesis, which are linked to cancer initiation and progression^{1–4,95,96}. Our work provides important context for understanding how Chk2 mutations, which are penetrant risk alleles for several types of cancer^{97–99}, influences disease initiation and progression.

This study highlights how well-characterized interphase signaling pathways, including Chk2 activation and G2/M cell cycle arrest by the DNA damage response pathway, are rewired in mitosis. While Chk2 activation in interphase strictly relies on activation by apical DNA damage response kinases^{32,59,63,64}, we identified that these proteins are



dispensable for the Chk2-PLK1 pathway described here. Instead, we describe how the nonreceptor tyrosine kinase JAK2, which canonically functions in innate immune signaling, is important for Chk2-mediated PLK1 activity. Our work builds on that of Chowdhury et al.⁴⁵ to show evidence of Chk2 activation and function independent of other members of the DNA damage response pathway.

The DNA damage response pathway antagonizes mitotic kinase activity in interphase by inactivating CDK1, Aurora A, and PLK1, but our work, along with the work of others^{43,47,100,101}, has demonstrated that this relationship is inverted in mitosis, where members of the DNA damage response pathway support mitotic kinase signaling. The molecular logic for this flipped relationship is incompletely understood but may be due

Fig. 4 | Chk2 inhibition and partial PLK1 inhibition induce mitotic defects.

A, B Left, representative image of prometaphase (**A**) or metaphase (**B**) RPE-1 cells stained for phospho-TCTP S46 (p-TCTP) following 1-h treatment with 5 nM BI-2536 (PLK1i), Chk2i (10 μ M BML-277), or a DMSO vehicle control. Images are single z-planes for each channel. Scale bar, 5 μ m. Right, quantification of prometaphase (**A**) or metaphase (**B**) p-TCTP signal taken from single z-slice. Each point represents one cell normalized to the average value in the DMSO condition for each replicate. Error bars SD of individual cell values combined from 3 experimental replicates, $n = 99$ DMSO prometaphase, $n = 95$ 5 nM PLK1i, $n = 48$ Chk2i prometaphase; $n = 89$ DMSO metaphase, $n = 66$ 5 nM PLK1i metaphase, $n = 40$ Chk2i metaphase. $*p < 0.05$, unpaired two-tailed *t*-test. **C** Left, representative image of U2OS cells with aligned or misaligned chromosomes. ACA anti-centromere antibody. Scale bar, 5 μ m. Right, quantification of misalignment rate in RPE-1 (left) or U2OS (right) cells following 1-h treatment with inhibitors or DMSO control. Error bars SD. Each point represents the

rate from an experimental replicate ($N = 3$). $*p < 0.05$, paired two-tailed ratio *t*-test of replicate values. **D** Representative z-projected images of U2OS cells with mitotic defects. Scale bar on large panels, 5 μ m. Inset scale bar, 1 μ m. **E** Quantification of mitotic defects in U2OS cells treated for 1 h with inhibitors or vehicle control. Each point represents the rate from an experimental replicate ($N = 3$). Error bars SD. $*p < 0.05$, paired two-tailed ratio *t*-test. ns not significant ($p > 0.05$). **F** Left, representative image of telophase RPE-1 cells stained for alpha tubulin and pericentrin following 1-h treatment inhibitors or a DMSO vehicle control. Images are maximum intensity z-projections for each channel. Scale bar, 5 μ m. Right, quantification of the rate of cytokinetic furrow formation. Each point represents the rate from an experimental replicate ($N = 5$ DMSO and Chk2i, $N = 4$ 5 nM PLK1i). Error bars SD. $*p < 0.05$, paired two-tailed ratio *t*-test. All panels, data are presented as mean values \pm SD. Source data are provided as a Source Data file.

in part to mitotic degradation of key players, including Bora and the CDK1-inhibiting kinase Wee1^{29,35}. Another possibility by which mitosis-specific signaling interactions may occur is that the spatial segregation of cytosolic and nuclear components in interphase is absent in mitosis. Nuclear envelope breakdown in early mitosis may allow for nuclear proteins, such as Chk2, to interact with cytoplasmic proteins, including JAK2 and PLK1, in a phase-specific manner. PLK1 is mostly cytosolic in interphase and translocates to the nucleus only when active¹⁰², thereby restricting the interaction between Chk2 and inactive cytosolic PLK1. After nuclear envelope breakdown, however, Chk2 is no longer spatially segregated from inactive PLK1 and may directly phosphorylate it to promote its activity.

We hypothesize that the rewired relationship between Chk2 and PLK1 in mitosis may trigger a switch between different modes of PLK1 regulation. The G2 activation of PLK1 by Aurora A-Bora is a highly sensitized “bistable switch” whereby both kinases promote the others’ activity, likely as a mechanism to ensure high activity and commitment to enter mitosis¹⁰³. This bistability, however, is lost in mitosis. Both by inhibiting Chk2 and through partial inhibition of PLK1 with low-dose PLK1 inhibitors, we observe that cells exhibit a stable and partial reduction in PLK1 activity. As PLK1 has been shown to negatively regulate Chk2 activity¹⁰⁴, this could be due to the switch from a positive feedback loop in G2 to a negative feedback relationship in mitosis. This negative regulation may be particularly important in contexts where PLK1 activity must be precisely fine-tuned, such as controlling kinetochore-microtubule attachments⁷, where both hyper- and hypo-activity negatively impact proper mitotic progression^{105–108}. We identified that the localization of both centrosome- and kinetochore-associated populations of PLK1 is reduced following treatment with Chk2i, suggesting to us that both populations could be regulated by Chk2. The relative contribution of Chk2 to these and other populations of PLK1, including the recently reported pool at the inner centromere¹⁰⁹, remains unclear.

PLK1 activity is not entirely abrogated, even in cases where we inhibit Chk2 and Aurora A in combination, prompting the hypothesis that there are other currently unknown pathways that sustain mitotic PLK1 activity. We speculate that there may be additional and currently unknown kinases that also act on PLK1 T210 in mitosis. It is also possible that phosphatases, possibly against PLK1 T210 and some PLK1 substrates, may be negatively regulated in contexts of low PLK1 activity to prevent their dephosphorylation. This is indeed an interesting question, and future publications should consider the complete network of proteins that regulate PLK1 activity. Together, our work shows that regulation of PLK1 in mitosis is more complex than previously appreciated and that a better understanding of the pathways that fine-tune PLK1 activity may identify therapeutic vulnerabilities for cancer treatment.

Methods

Cell lines and culture medium

U2OS (ATCC, HTB-96), RPE-1 hTERT (ATCC, CRL-4000), RPE-1 hTERT asPLK1-GFP (gift from Burkard lab), HeLa (Abcam, ab255928), PANC-1

(ATCC, CRL-1469), HeLa H2B-GFP (Sigma-Aldrich sccl17), and 293 T (ATCC, CRL-3216) cells were cultured in Dulbecco’s modified Eagle’s medium (DMEM; Gibco) supplemented with 10% fetal bovine serum (FBS; Gibco) and 1% penicillin/streptomycin (P/S) (Gibco). HCT-116 (ATCC, CRL-247) cells were cultured in McCoy’s 5A medium (ATCC 30-2007) supplemented with 10% FBS and 1% P/S. A549 WT (Abcam, ab275463) and Chk2 knockout cells (Abcam, ab276098) were grown in Ham’s F-12K Kaighn’s Modification (Gibco 21127-022) supplemented with 10% FBS and 1% P/S. All cells were cultured at 37 °C with 5% CO₂. HCT-116 cells stably expressing the Chk2 rescue construct were cultured in the presence of 0.5 mg/ml Geneticin (G418, Gibco 10131-027). Forty-eight hours prior to drug sensitivity assays, cells were grown in media without selection agents. No commonly misidentified cell lines were used in this study.

Cell transfection

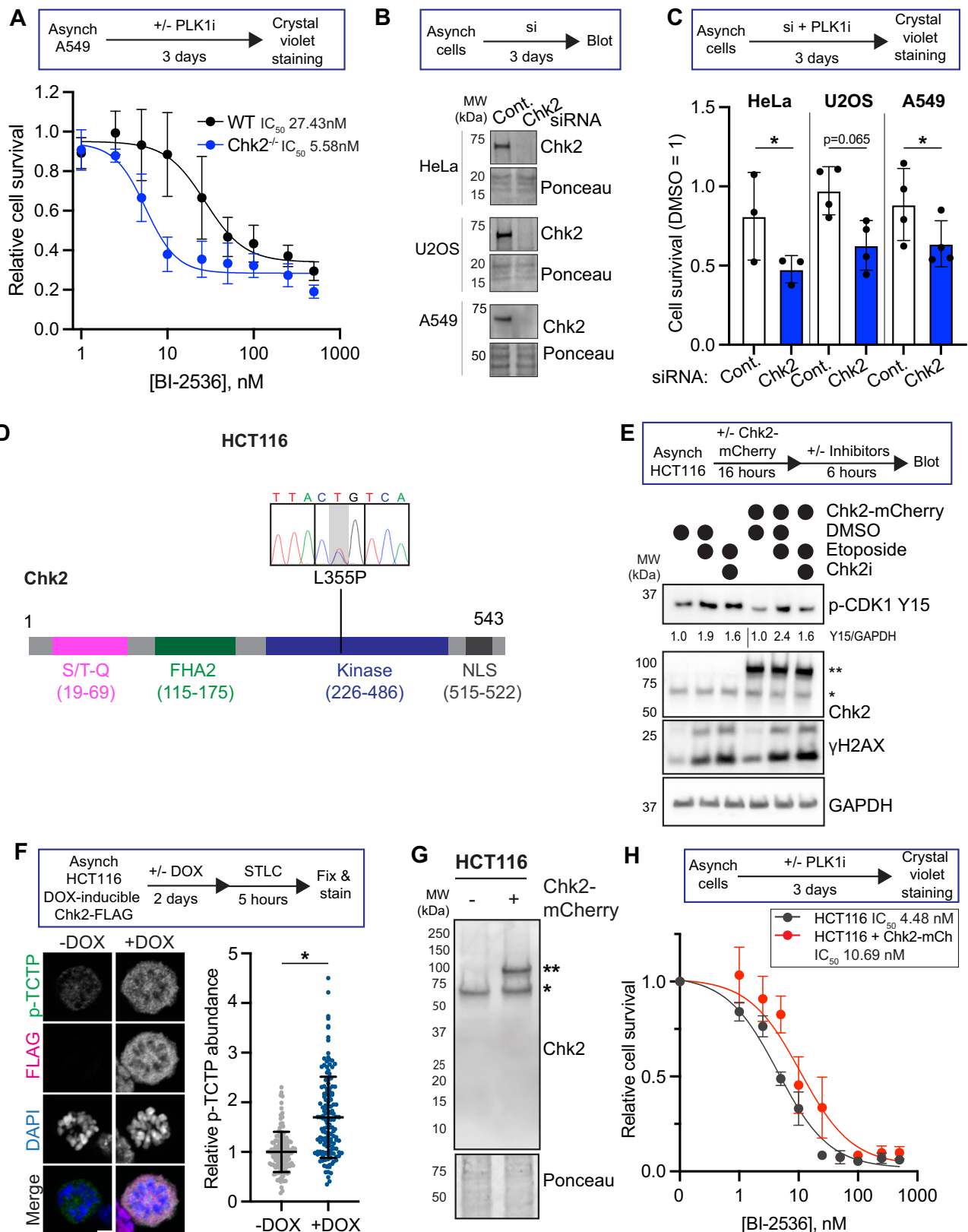
All cells were transfected with plasmids using the Lipofectamine™ 3000 Transfection Reagent (Invitrogen) according to manufacturer instructions. siRNA experiments were performed by transfection of either the *Silencer™* Select Negative Control No. 1 siRNA (ThermoFisher, item number 4390843) or *Silencer™* Select Pre-designed Chk2 siRNA (ThermoFisher, item number 119278) using the Lipofectamine™ RNAiMAX Transfection Reagent (Invitrogen) according to manufacturer instructions. 1 pmol of siRNA was transfected per 96 well for viability experiments and 25 pmol of siRNA was transfected per 6 well. plk1 T210A was a gift from Michael Yaffe (Addgene plasmid # 132965; <http://n2t.net/addgene:132965>; RRID:Addgene_132965). plk1 WT GFP-myc was a gift from Michael Yaffe (Addgene plasmid # 132963; <http://n2t.net/addgene:132963>; RRID:Addgene_132963).

Viral infection

Doxycycline-inducible 3X-FLAG Chk2 lentivirus was generated via co-transfection of 293 T cells with pSLIK_neo_3xflag_CHEK2, which was a gift from Kevin Janes (Addgene plasmid #136536; <http://n2t.net/addgene:136536>; RRID:Addgene_136536), pCMV dR8.2 dvpr (Addgene 8455, gift from Bob Weinberg), and pCMV-VSV-G (Addgene 8454, gift from Bob Weinberg) using Lipofectamine™ 3000 Transfection Reagent (Invitrogen) according to manufacturer instructions. Viral supernatant was harvested 3 days after transfection and added to HCT-116 cells cultured in McCoy’s 5A supplemented with 1% P/S, 10% FBS, and 8 μ g/mL polybrene infection/transfection reagent (Sigma-Aldrich). HCT-116 cells were selected and grown in the presence of 0.5 mg/ml Geneticin (G418, Gibco 10131-027).

Western blotting

Cells were collected for blotting by either collecting non-adherent shaken-off mitotic cells or by trypsinization (interphase cells). Cells were spun down, washed 1 \times with PBS, and then resuspended in 1 \times SDS Sample Buffer (0.05 M Tris-HCl pH 6.8, 440 mM sucrose, 3% sodium dodecyl sulfate, 0.01% Bromophenol blue, 10%



beta-mercaptoethanol). The protein samples were lysed with an insulin syringe and boiled at 95°C for 15 min before being run on an SDS-Page gel. 50 μM PhosTag acrylamide (FUJIFILM Wako Chemicals USA Corporation) within hand-cast 7.5% acrylamide gels was used to separate phosphorylated PLK1 (Supplementary Figs. 7F, 8A). Gels were run in 1× MES buffer (Invitrogen NP0002) with the exception of

PhosTag gels, which were run in 1× tris glycine SDS buffer (BioRad). Protein gels were transferred to 0.45 μm nitrocellulose membranes using the Trans-Blot Turbo Transfer System (Bio-Rad). Membranes were stained with Ponceau S staining solution (0.5% (w/v) Ponceau S, 1% glacial acetic acid) to visualize total protein loading, imaged, and then Ponceau was removed by washing with 1× Tris-Buffered

Fig. 5 | Chk2 deficiency sensitizes cells to PLK1 inhibition. **A** Top, experimental setup. Bottom, relative cell viability (DMSO = 1) measured by crystal violet following 3-day treatment with PLK1 inhibitor BI-2536. Points represent average of $N = 4$ experimental replicate values averaged from technical triplicates. Error bars SEM of replicate averages. **B** Representative blots of cells treated for 3 days with either a nontargeting siRNA (control) or siRNA against Chk2 in HeLa, U2OS, and A549 cells. **C** Quantification of cell viability following siRNA treatment and 2.27 nM BI-2536. Each point marks the mean of $N = 3$ HeLa, $N = 4$ U2OS and A549 experimental replicates, each averages from technical triplicates and normalized to DMSO-treated cells. Error bars SD of experimental replicates. $p = 0.049$ HeLa, $p = 0.065$ U2OS, $p = 0.0176$ A549 ratio paired two-tailed t -test of replicate mean values. **D** Map of Chk2 protein with indicated domains including S/T-Q cluster, FHA2, kinase, and nuclear localization sequence (NLS). Top, trace file of *Chk2* locus from HCT-116 cells. Gray shading indicates the heterozygous L355P mutation. **E** Top, experimental setup. Bottom, representative western blot of HCT-116 cells with or without Chk2-mCherry challenged with etoposide (Etop, 10 μ M) or in combination with

Chk2i (10 μ M BML-277) for 6 h. Numbers are quantification of p-Y15 signal normalized to GAPDH loading control and to DMSO-treated condition. This experiment has been repeated 1 other time with similar results. **F** Left, quantification of p-TCTP abundance in STLC-arrested HCT-116 cells transduced with a doxycycline (DOX)-inducible 3xFLAG-Chk2 construct. Cells were either treated with 0.1 μ M DOX or untreated for 48 h prior to STLC addition. Each point represents one cell normalized to the average value in the untreated condition for each replicate. Error bars SD of individual cell values combined from $N = 3$ experimental replicates, $n = 131$ -DOX, $n = 141$ +DOX. $*p < 0.05$, two-tailed t -test of replicate mean values. Right, representative immunofluorescence image. Scale bar, 5 μ m. **G** Representative western blot of HCT-116 cells with or without expression of the Chk2-mCherry rescue construct. **H** Quantification of relative cell viability in HCT-116 cells following 3-day treatment with BI-2536 titration. Points represent average of 3–4 experimental replicate values averaged from technical triplicates. Error bars SEM of replicate averages. Source data are provided as a Source Data file.

Saline + 0.1% Tween-20 (TBS-T). Membranes were blocked with TBS-T + 5% bovine serum albumin (BSA) or 5% milk for at least 1 h at room temperature with gentle rocking. Primary antibodies were diluted in blocking solution, then added to membranes to incubate overnight at 4 °C with gentle agitation. Membranes were washed 3× with TBS-T for 5 min before incubation with secondary antibody. Secondary antibodies conjugated to with fluorophores or horseradish peroxidase (HRP) were diluted 1:5000 in 1% BSA and added to membranes for at least 1 h at room temperature, followed by 2 additional washes to remove unbound secondary antibody. Membranes were incubated with Clarity Western ECL substrate (for HRP-conjugated antibodies; Bio-Rad) and imaged on the ChemiDoc MP Imaging system (Bio-Rad).

Immunofluorescence

Cells were grown on coverslips and treated with the indicated drugs, then fixed with 3.5% paraformaldehyde for 15 min, permeabilized with phosphate buffered saline (PBS) + 1% Triton X-100 for 15 min and blocked with PBS + 1% BSA for 10 min. Coverslips were then incubated with primary antibody diluted in PBS + 1% BSA at 4 °C overnight. Coverslips were then washed with PBS to remove unbound primary antibody. Secondary antibodies conjugated to fluorophores and 1 mg/mL DAPI were diluted 1:1000 in PBS + 1% BSA before being added to coverslips for 1 h at room temperature. Cells were washed again with PBS and mounted onto glass slides using ProLong Gold Antifade Mountant (Invitrogen) and left to dry overnight. All images were acquired on a Nikon ECLIPSE Ti2 W2 spinning disk confocal microscope with a Hamamatsu Fusion sCMOS camera. Image acquisition was managed using NIS-Elements (Nikon).

Fluorescence and western blot quantification

All images were analyzed in Fiji. For western blot quantification, regions of interest were drawn around the band and the area and mean gray value for each band was recorded. A mean gray value for the background in a negative space immediately adjacent to the band was also recorded. The value for each band was calculated by subtracting the mean gray value for the background from the mean gray value for the band and then multiplying that background-subtracted value by the band's area. All values were then normalized to similarly background-subtracted values in Ponceau S staining (unless otherwise indicated), normalized to the control, and graphed. Similarly, immunofluorescence values were calculated by measuring the fluorescence intensity for an area of interest and then subtracting out a mean gray value picked from a region without cells. For p-TCTP S46 immunofluorescence, a no primary control coverslip was imaged alongside experimental samples, and the average gray value from >5 mitotic cells on the no primary control was the subtracted background value for experimental samples.

FRET

Plk1 FRET sensor c-jun substrate was a gift from Michael Lampson (Addgene plasmid #45203; <http://n2t.net/addgene:45203>; RRI-D:Addgene 45203). The sensor is untargeted with no obvious localization to mitotic structures. Cells were transiently transfected with a and plated onto glass-bottom plates. The next day, cells were arrested in nocodazole for 4 hours prior to imaging. Live-cell imaging was performed with a heated stage at 37 °C and 5% CO₂. CFP, YFP, FRET, and brightfield images were taken for each cell prior to addition of drugs. After initial image acquisition, the media for each condition was replaced with fresh media containing nocodazole and DMSO or a small-molecule inhibitor against the kinase of interest. Imaging was resumed for 1 h after addition of drugs. CFP/FRET ratios were calculated by subtracting background values for FRET and CFP at both the initial timepoint (T_0 , before addition of inhibitors) and the final timepoint (T_{60} , 1 h) and calculating $(CFPt_{60}/FRETt_{60})/(CFPt_0/FRETt_0)$. Ratio values were then normalized so that the mean CFP/FRET ratio change after 1 h for the DMSO condition equals 1. Biological replicates were performed using the same imaging conditions within each replicate but varied between replicates. Replicates were then combined, and individual cell values are plotted.

Live-cell imaging

For the live-cell imaging of chromosome segregation defects (Supplementary Fig. 11D), asynchronous HeLa cells stably expressing H2B-GFP were cultured in a 24-well glass-bottom dish (Cellvis). The dish was mounted on a Tokai Hit STX stage-top incubator (Spectra Services) to maintain an imaging environment of 37 °C with 5% CO₂. Z-stacks were taken at 60× for each cell with a range of 8 μ m at 1 μ m steps. We identified prophase cells that displayed chromatin compaction and individualization but had not congressed around the mitotic spindle. Initial images of the cell in DIC and 488 image were taken, and then the media was replaced with fresh media containing 10 μ M Chk2i, 5 nM BI-2536, 5 μ M JAK2i, or an equal volume DMSO control. The remaining images were taken at 5-minute intervals over 2.5 hours. For the measurement of cytokinesis (Supplementary Fig. 11G), BioTek Cytation 5 Cell Imaging Multimode Reader (Agilent) was used. All imaging was performed at 37 °C with 5% CO₂. Images were taken with a 40× objective at 2.5-min intervals, 7 μ m stack with 1 μ m step.

PLK1 immunoprecipitation

Following nocodazole arrest and inhibitor treatment, U2OS cells were washed with ice-cold dPBS (Gibco) and lysed in lysis buffer (20 mM HEPES [pH 7.4], 150 mM KCl, 10% glycerol, 5 mM DTT, 1% Triton X-100, 1 Pierce Protease Inhibitor Tablet [EDTA-free], and 1 phosphatase inhibitor PhosSTOP™ Roche tablet). Crude cell extract was lysed with an insulin syringe and pre-cleared by incubation with 3 μ g Normal Rabbit IgG (Cell Signaling Technology) and 10 μ L Pierce™ Protein A/G

Magnetic Beads (Thermo Scientific 88803) with constant rotation at 4 °C for 4 h. The beads were removed with centrifugation at 23000 rcf for 1 min. The remaining pre-cleared cell extract was incubated overnight with 5 µg of Rabbit Anti-PLK1 antibody (Millipore) with constant rotation at 4 °C. 25 µL of Protein A/G Magnetic Beads were added to the suspension and samples were incubated for an additional 4 h at 4 °C with constant rotation. The beads were washed 5 times with Lysis Buffer and vortexing and were then eluted SDS elution buffer (50 mM Tris-HCl [pH 8.0], 1 mM EDTA [pH 8.0], 1% SDS). Immunoprecipitated protein was eluted at 95 °C for 10 min. Samples were diluted with 2× Sample Buffer and prepared for western blotting as described above.

Chk2 purification

Wild-type and analog-sensitive Chk2 ORF sequences were cloned in the pGex6p-1 plasmid (Genscript, see plasmid construction section for details) and transformed into BL21 bacterial cells (New England Biolabs). Protein expression was induced by growing a dense overnight culture, diluting to an OD₆₀₀ value of 0.1, growing the culture until OD₆₀₀ equals 0.4, and then adding 1 mM IPTG (Bio Basic item number 367-93-1) for 4 h at 37 °C with shaking. Cells were collected by centrifugation and frozen at −80 °C. Cells were resuspended in 10 mLs chilled lysis buffer (50 mM tris PH 7.4, 150 mM NaCl, 1 mM DTT, 50 mM NaF, 5 mM EDTA, 1% glycerol supplemented with protease inhibitor tablet (Pierce), pH adjusted to 7.6) and sonicated to lyse. The lysate was then centrifuged at 45,000 × g for 20 min at 4 °C, and the soluble fraction was collected for Chk2 affinity purification. Chk2 was immunoprecipitated from the soluble fraction by addition of Glutathione-conjugated magnetic agarose beads (Pierce 78601) overnight with gentle rocking. After thorough washing in ice cold cleavage buffer (50 mM tris pH 7, 150 mM NaCl, 1 mM DTT), Chk2 was eluted from the beads by addition of PreScission Protease (Genscript Z02799) overnight rocking at 4 °C. Finally, the protease was trapped on the beads by addition of additional GST conjugated beads and 1 hour incubation with rocking at 4 °C. The GST beads were isolated with a magnet, and purified Chk2 was collected in the supernatant and combined 1:1 with freezing buffer (100 mM tris, 300 mM NaCl, 10 mM DTT, 82% glycerol) and stored at −80 °C in single-use aliquots.

ADP-Glo™

ADP-Glo™ (Promega) was performed according to manufacturer instructions. Briefly, kinase reactions were performed with 10–100 ng of the kinase of interest (optimized for each kinase) and 0.5 µg Chk2 substrate (derived from human CDC25C protein isoform A amino acids 205–225, used in Chk2 kinase reactions) or Casein, PLK1 and Aurora A substrate, in manufacturer kinase reaction buffer (40 mM tris pH 7.5, 20 mM MgCl₂, 0.1 mg/mL BSA, 1 mM DTT, and 100 µM ATP) at 30 °C for 30 min with shaking with indicated concentrations of inhibitor or DMSO control. A control reaction with no enzyme was also included. The reaction was then cooled to room temperature and incubated with equal volume of ADP Glo reagent for 40 min before then being incubated with kinase detection reagent for 1 h. Reactions were transferred to a 384 well plate and luminescence was recorded on a BioTek Synergy HI microplate reader with an integration time of 0.5 ms. Values recorded for the substrate-only reaction were subtracted from experimental values, and these subtracted experimental values were normalized to vehicle control (DMSO) reactions. Reactions were performed in at least three experimental replicates.

In vitro kinase assays & recombinant proteins

GST-Chk2 used in Supplementary Figs. 3A and 8D was purchased from Promega (V4020). HIS-PLK1 used in ADP-Glo was from Promega (V2841). HIS-PLK1 used in Fig. 3D and S8D in vitro reactions was from Abcam (AB51426-1002). HIS-Aurora A was purchased from Abcam

(AB42595). Wild-type or T383A T387A kinase-dead MBP-Chk2-6xHIS was a gift from Jesse Reinhardt lab⁸⁰. HIS-CDK1-Cyclin B1 was purchased from ThermoFisher Scientific (PV3980). Details of individual in vitro kinase reactions are described in the corresponding figure captions. Curve fit for in vitro kinase assay inhibitor IC₅₀ calculations were calculated with nonlinear regression with standard slope, equal to a Hill slope of −1.0. All kinase reactions were performed in kinase assay buffer (20 mM 3-morpholinopropane-1-sulphonic acid (MOPS), pH 7.2, 25 mM MgCl₂, 500 µM ATP, 1 mM DTT) at 30 °C with gentle agitation. Following incubation, reactions were quenched by adding EDTA to a final concentration of 5 mM before being analyzed by immunoblotting. Reactions to be analyzed by mass spectrometry were flash-frozen in liquid nitrogen. Lambda phosphatase treatment was according to manufacturer instructions (NEB P0753S).

Parallel reaction monitoring (PRM) quantification of the phosphorylation site

The Orbitrap Fusion Lumos Tribrid based mass spectrometer MS (Thermo Fisher Scientific) was used for the targeted proteomic measurement using the Parallel Reaction Monitoring (PRM) mode¹¹⁰. And Skyline¹¹¹ was used to visualize and report the results. Briefly, gel bands were processed by following a standard protocol¹¹² with trypsin (Promega) digestion at a 10 ng/µL concentration overnight. After C18 purification, the digest peptides from DMSO and Chk2 conditions were respectively spiked with the synthetic lysine-labelled heavy phospho-peptide of(phos)TLC(Carbamidomethylation)GTPNYIA-PEVLSK (+8 Da) that was synthesized by Thermo Fisher Scientific. The resulting samples were injected into MS, in which PRM measurement was performed to confirm the endogenous phospho-peptide identity and for the relative quantification, using 500 fmol of the heavy phospho-peptide as the reference. The theoretical peptide precursor m/z values of the light and heavy versions used in PRM analysis were generated by Skyline. The isolation window was set to be 1.4 m/z. The Orbitrap resolution for PRM was set at 30,000, AGC target 1.0e5, and maximum injection time 150 ms¹¹³. A stepped higher energy collisional dissociation collision energy of 2% (centered at 28%) was used. The resultant PRM data were imported into Skyline for manual inspection and quantification.

Plasmid construction

The plasmids generated in the study are Chk2 WT and analog-sensitive (L301G) in an N-terminal constitutive mCherry mammalian expression vector and pGEX-6p-1, an inducible bacterial expression vector. The open reading frame of wild-type Chk2 was subcloned by amplifying the open reading frame of Chk2 from pSLIK_neo_3xflag_CHEK2, which was a gift from Kevin Janes (Addgene plasmid #136536; <http://n2t.net/addgene:136536>; RRID:Addgene_136536). Constructs were validated with Sanger sequencing before use. The analog-sensitive L301G mutation in Chk2 was generated by site-directed mutagenesis where nonoverlapping primers (TTATATTGTTGGGAATTGATGGAAGG, FW; TAATCTTCTGCATCAAAAAAG, RV) introducing the single-nucleotide change were used to amplify the mCherry-wtChk2 sequence, then were phosphorylated by polynucleotide kinase (PNK) and ligated together using T4 DNA ligase. Mutation was confirmed via sequencing (sequencing primer GGAAGTGGTGCCTGTGGAGAG).

Cell line genotyping

DNA was extracted from HCT-116, A549 WT, and A549 Chk2^{−/−} cells using the Monarch® Genomic DNA Purification Kit (NEB). Prior to Sanger sequencing, regions surrounding the putative mutation sites were amplified using Phusion High-Fidelity polymerase (NEB) with the below primers: Chk2 KO Seq F (GTCGTGATGTCTCGGAGTCG-GATG), Chk2 KO Seq R (TGACGCCACTTGCTCAGGCCTGCTC), Chk2 L355 F (GGAGAATATGGTTGTGTGTATCACGGCTTA), Chk2 L355 R (GGTCACTTGACACAACAGAGCTCAA).

Antibodies

Antibodies used for this study were: human anti-centromere antisera (ACA) (Antibodies Inc., 15-234-0001), alpha tubulin (Cell Signaling Technology, 3873), Chk2 (Cell Signaling Technology, 3440), cyclin B1 (Cell Signaling Technology, 12231), FLAG (Sigma-Aldrich F1804), GAPDH (Santa Cruz Biotechnology sc32233), phospho-Aurora A/B/C (Cell Signaling Technology D13A11), phospho-CDK1 Y15 (Fortis Life Sciences BLR101H), pericentrin (Abcam ab4448), PLK1 mouse (used in all western blots except for PhosTag, Millipore 05-844), PLK1 rabbit (used in Phos-tag gel, PLK1 IP, and PLK1 immunofluorescence in Supplementary Fig. 10C; Millipore ABE2619), phospho-PRC1 T481 (Abcam ab62366 used in Supplementary Fig. 7; Invitrogen PA5-106104 used in Fig. 3A), phospho-TCTP (Cell Signaling Technology 5251), R-X-X-phosphoS/T (Cell Signaling Technology 9614), TCTP (Cell Signaling Technology 5128), γ H2AX (Novus NB100-74435), phospho-PLK1 T210 D5H7 (Cell Signaling Technology 9062), phospho-PLK1 T210 5472 (Cell Signaling Technology), phospho-Chk2 S33/35 (Cell Signaling Technology 2665), phospho-Chk2 T383 (Thermo Fisher Scientific PA5-37786), lamin A/C (Cell Signaling Technology 4777S), TPE (Abcam ab92570), p53 (Santa Cruz sc-126), p-Chk1 S317 (Cell Signaling Technology 12302S), tubulin (Cell Signaling Technology 3873S).

Inhibitors and small molecule reagents

Nocodazole (Cayman 13857100 ng/mL), BI-2536 (Cayman 17388, concentration as indicated), BML-277 (EMD Millipore Corp 220486, concentrations as indicated), 3-MB-PP1 (EMD Millipore Corp. 529582, concentrations as indicated), S-trityl-L-cysteine (STLC, Sigma Aldrich 164739, 10 μ M), Doxorubicin (DOXO, TCI D4193, 2 μ M), Etoposide (Etop, Cayman 12092, 10 μ M), MLN8237 (Aurora A inhibitor, Cayman 13602, 50 nM), RO-3306 (CDK1 inhibitor, Cayman 15149, 5 μ M), MG132 (EMD Millipore Corp, 474790, 20 μ M), doxycycline (DOX, Alfa Aesar J67043), ATMi (KU55933, Cayman 16336, 10 μ M), DNA-PKi (M3814, Selleckchem S8586, 5 μ M), ATRi (AZ20, ChemCruz sc-503186, 10 μ M), JAK2i (JAK2 inhibitor IV, Thermoscientific j65506, 5 μ M), okadaic acid (OA, 100 nM), Chk2i 1 (3.4 μ M, Millipore 220485), p-nitrobenzyl mesylate (PNBM, 2.5 mM, Abcam ab138910), N6-Benzyl-ATP- γ S (10 μ M, Jena Biosciences NU-241), GSK923295 (CENP-Ei, 2 μ M, 1088965-37-0 Med Chem Express), Reversine (MPS1i, 1 μ M Cayman Chemical 10004412).

Analog-sensitive PLK1 labelling

RPE-1 cells expressing asPLK1-GFP were arrested in mitosis using 100 ng/mL nocodazole, then isolated via shake off, and treated with 50 μ M 3-MB-PP1, 10 μ M Chk2i, or a DMSO control for 1 h. Cells were then collected via centrifugation and resuspended in hypotonic lysis buffer (16 mM Hepes pH 7.4, 10 mM KOAc, 0.5 mM MgOAc, 0.1 mM DTT). Cells were lysed on ice with an insulin syringe for 5 min. The kinase reaction was prepared on ice by combining 50 μ g of cell lysate with 20 mM 3-morpholinopropane-1-sulphonic acid (MOPS), pH 7.2, 25 mM MgCl₂, 2 mM GTP, 500 μ M unlabeled ATP, 10 μ M N6-Benzyl-ATP- γ S, 0.1 mM DTT, and 50 μ M 3-MB-PP1, 10 μ M Chk2i, or a DMSO control. The reaction was performed for 15 min at 30 °C with constant shaking and quenched with 50 mM EDTA. To alkylate the reaction, we added 2.5 mM PNBM for 2 h at room temperature. Samples were then combined with sample buffer and thiophosphorylated proteins were detected by western blotting with the thiophosphate ester (TPE) antibody.

Drug sensitivity

Following plating in a 96-well plate, cells were treated in technical triplicates with inhibitors or an equal volume of DMSO for 3 days. Cells were washed thoroughly with PBS and then fixed and stained using crystal violet (0.5 g per 100 mL 20% methanol) for 1 min. Cells were washed with 2 \times with water and crystal violet was measured using BioTek Synergy H1 microplate reader by measuring absorbance at 570 nm. For each replicate, technical triplicate values for each drug

concentration were averaged. Data plotted represents the technical triplicate averaged value for each replicate. All data shown represent at least 3 independent biological replicates. Curve fit for cell viability IC₅₀ calculations were calculated using nonlinear regression model with variable slope.

Scoring mitotic defects

All mitotic defects were scored on fixed and stained coverslips. Lagging chromosomes were called when there was a DNA fragment (DAPI) that was also positive for ACA (acentromere antibody) that was visibly isolated from the chromosome masses. DAPI signal that was ACA-negative was classified as acentric chromatin, and DAPI signal that was continuous between the segregating masses, regardless of ACA signal, was called as a chromosome bridge.

Statistics and reproducibility

For assays where individual points per cell are recorded, such as immunofluorescence and FRET, values from within a replicate were first tested for outliers using the ROUT test where $Q=1\%$. After removing outliers, values were normalized to the average value of the vehicle control. Unless otherwise indicated, statistics are performed on the average of the normalized replicate values using a two-tailed t -test. In places where multiple comparisons are performed, we used one-way ANOVA with Bonferroni's correction. All p values can be found in the Source Data file. No statistical method was used to predetermine sample size. Data were excluded from analysis only in experimental replicates where positive controls failed to change in line with well-established expectations from prior literature, such as the reduction of p-Chk1 following ATR inhibition. The experiments were not randomized. The investigators were not blinded to allocation during experiments and outcome assessment.

Reporting summary

Further information on research design is available in the Nature Portfolio Reporting Summary linked to this article.

Data availability

All data and unique reagents generated for this manuscript are available upon reasonable request. Raw data for western blots, immunofluorescence, and sequencing can be found on [FigShare](#). The mass spectrometry data have been all deposited to the ProteomeXchange Consortium via the PRIDE [PXD053933](#). Source data are provided with this paper.

References

1. Lee, A. J. et al. Chromosomal instability confers intrinsic multidrug resistance. *Cancer Res.* **71**, 1858–1870 (2011).
2. Bakhoum, S. F. et al. Chromosomal instability drives metastasis through a cytosolic DNA response. *Nature* **553**, 467–472 (2018).
3. Nowak, M. A. et al. The role of chromosomal instability in tumor initiation. *Proc. Natl Acad. Sci. USA* **99**, 16226–16231 (2002).
4. Umbreit, N. T. et al. Mechanisms generating cancer genome complexity from a single cell division error. *Science* **368**, eaba0712 (2020).
5. van Vugt, M. A. et al. Polo-like kinase-1 is required for bipolar spindle formation but is dispensable for anaphase promoting complex/Cdc20 activation and initiation of cytokinesis. *J. Biol. Chem.* **279**, 36841–36854 (2004).
6. Burkard, M. E. et al. Chemical genetics reveals the requirement for Polo-like kinase 1 activity in positioning RhoA and triggering cytokinesis in human cells. *Proc. Natl Acad. Sci. USA* **104**, 4383–4388 (2007).
7. Liu, D., Davydenko, O. & Lampson, M. A. Polo-like kinase-1 regulates kinetochore-microtubule dynamics and spindle checkpoint silencing. *J. Cell Biol.* **198**, 491–499 (2012).

8. Lera, R. F. & Burkard, M. E. High mitotic activity of Polo-like kinase 1 is required for chromosome segregation and genomic integrity in human epithelial cells. *J. Biol. Chem.* **287**, 42812–42825 (2012).
9. Sana, S., Keshri, R., Rajeevan, A., Kapoor, S. & Kotak, S. Plk1 regulates spindle orientation by phosphorylating NuMA in human cells. *Life Sci. Alliance* **1**, e201800223 (2018).
10. Ohta, M. et al. Polo-like kinase 1 independently controls microtubule-nucleating capacity and size of the centrosome. *J. Cell Biol.* **220**, e202009083 (2021).
11. Lera, R. F. et al. Plk1 protects kinetochore-centromere architecture against microtubule pulling forces. *EMBO Rep.* **20**, e48711 (2019).
12. Haren, L., Stearns, T. & Luders, J. Plk1-dependent recruitment of gamma-tubulin complexes to mitotic centrosomes involves multiple PCM components. *PLoS ONE* **4**, e5976 (2009).
13. Lenart, P. et al. The small-molecule inhibitor BI 2536 reveals novel insights into mitotic roles of polo-like kinase 1. *Curr. Biol.* **17**, 304–315 (2007).
14. McKinley, K. L. & Cheeseman, I. M. Polo-like kinase 1 licenses CENP-A deposition at centromeres. *Cell* **158**, 397–411 (2014).
15. Elia, A. E., Cantley, L. C. & Yaffe, M. B. Proteomic screen finds pSer/pThr-binding domain localizing Plk1 to mitotic substrates. *Science* **299**, 1228–1231 (2003).
16. Kang, Y. H. et al. Self-regulated Plk1 recruitment to kinetochores by the Plk1-PBIP1 interaction is critical for proper chromosome segregation. *Mol. Cell* **24**, 409–422 (2006).
17. Watanabe, N. et al. Deficiency in chromosome congression by the inhibition of Plk1 polo box domain-dependent recognition. *J. Biol. Chem.* **284**, 2344–2353 (2009).
18. Lera, R. F. et al. Decoding Polo-like kinase 1 signaling along the kinetochore-centromere axis. *Nat. Chem. Biol.* **12**, 411–418 (2016).
19. Elia, A. E. et al. The molecular basis for phosphodependent substrate targeting and regulation of Plks by the Polo-box domain. *Cell* **115**, 83–95 (2003).
20. Normandin, K. et al. Genetic enhancers of partial PLK1 inhibition reveal hypersensitivity to kinetochore perturbations. *PLoS Genet.* **19**, e1010903 (2023).
21. Hutterer, A. et al. Mitotic activation of the kinase Aurora-A requires its binding partner Bora. *Dev. Cell* **11**, 147–157 (2006).
22. Seki, A., Coppinger, J. A., Jang, C. Y., Yates, J. R. & Fang, G. Bora and the kinase Aurora a cooperatively activate the kinase Plk1 and control mitotic entry. *Science* **320**, 1655–1658 (2008).
23. Vigneron, S. et al. Cyclin A-cdk1-dependent phosphorylation of bora is the triggering factor promoting mitotic entry. *Dev. Cell* **45**, 637–650.e637 (2018).
24. Tavernier, N. et al. Bora phosphorylation substitutes in trans for T-loop phosphorylation in Aurora A to promote mitotic entry. *Nat. Commun.* **12**, 1899 (2021).
25. Macurek, L. et al. Polo-like kinase-1 is activated by aurora A to promote checkpoint recovery. *Nature* **455**, 119–123 (2008).
26. Jang, Y. J., Ma, S., Terada, Y. & Erikson, R. L. Phosphorylation of threonine 210 and the role of serine 137 in the regulation of mammalian polo-like kinase. *J. Biol. Chem.* **277**, 44115–44120 (2002).
27. Gheghiani, L., Loew, D., Lombard, B., Mansfeld, J. & Gavet, O. PLK1 activation in late G2 sets up commitment to mitosis. *Cell Rep.* **19**, 2060–2073 (2017).
28. Inoue, D. & Sagata, N. The Polo-like kinase Plx1 interacts with and inhibits Myt1 after fertilization of *Xenopus* eggs. *EMBO J.* **24**, 1057–1067 (2005).
29. Watanabe, N. et al. M-phase kinases induce phospho-dependent ubiquitination of somatic Wee1 by SCFbeta-TrCP. *Proc. Natl Acad. Sci. USA* **101**, 4419–4424 (2004).
30. O'Connell, M. J., Raleigh, J. M., Verkade, H. M. & Nurse, P. Chk1 is a wee1 kinase in the G2 DNA damage checkpoint inhibiting cdc2 by Y15 phosphorylation. *EMBO J.* **16**, 545–554 (1997).
31. Chaturvedi, P. et al. Mammalian Chk2 is a downstream effector of the ATM-dependent DNA damage checkpoint pathway. *Oncogene* **18**, 4047–4054 (1999).
32. Melchionna, R., Chen, X. B., Blasina, A. & McGowan, C. H. Threonine 68 is required for radiation-induced phosphorylation and activation of Cds1. *Nat. Cell Biol.* **2**, 762–765 (2000).
33. Evers, P. A., Erikson, E., Chen, L. G. & Maller, J. L. A novel mechanism for activation of the protein kinase Aurora A. *Curr. Biol.* **13**, 691–697 (2003).
34. Evers, P. A. & Maller, J. L. Regulation of *xenopus* Aurora A activation by TPX2. *J. Biol. Chem.* **279**, 9008–9015 (2004).
35. Chan, E. H., Santamaria, A., Sillje, H. H. & Nigg, E. A. Plk1 regulates mitotic Aurora A function through betaTrCP-dependent degradation of hBora. *Chromosoma* **117**, 457–469 (2008).
36. Bruinsma, W., Macurek, L., Freire, R., Lindqvist, A. & Medema, R. H. Bora and Aurora-A continue to activate Plk1 in mitosis. *J. Cell Sci.* **127**, 801–811 (2014).
37. Yamashiro, S. et al. Myosin phosphatase-targeting subunit 1 regulates mitosis by antagonizing polo-like kinase 1. *Dev. Cell* **14**, 787–797 (2008).
38. Cordeiro, M. H., Smith, R. J. & Saurin, A. T. Kinetochore phosphatases suppress autonomous Polo-like kinase 1 activity to control the mitotic checkpoint. *J. Cell Biol.* **219**, e202002020 (2020).
39. Wang, L., Guo, Q., Fisher, L. A., Liu, D. & Peng, A. Regulation of polo-like kinase 1 by DNA damage and PP2A/B55alpha. *Cell Cycle* **14**, 157–166 (2015).
40. Stolz, A. et al. The CHK2-BRCA1 tumour suppressor pathway ensures chromosomal stability in human somatic cells. *Nat. Cell Biol.* **12**, 492–499 (2010).
41. Stolz, A., Ertych, N. & Bastians, H. Loss of the tumour-suppressor genes CHK2 and BRCA1 results in chromosomal instability. *Biochem. Soc. Trans.* **38**, 1704–1708 (2010).
42. Shang, Z. et al. DNA-PKcs activates the Chk2-Brc1 pathway during mitosis to ensure chromosomal stability. *Oncogenesis* **3**, e85 (2014).
43. Petsalaki, E. & Zachos, G. Chk2 prevents mitotic exit when the majority of kinetochores are unattached. *J. Cell Biol.* **205**, 339–356 (2014).
44. Yeh, C. W., Yu, Z. C., Chen, P. H., Cheng, Y. C. & Shieh, S. Y. Phosphorylation at threonine 288 by cell cycle checkpoint kinase 2 (CHK2) controls human monopolar spindle 1 (Mps1) kinetochore localization. *J. Biol. Chem.* **289**, 15319–15327 (2014).
45. Chowdhury, M. A. N. et al. JAK2-CHK2 signaling safeguards the integrity of the mitotic spindle assembly checkpoint and genome stability. *Cell Death Dis.* **13**, 619 (2022).
46. McKinley, K. L. & Cheeseman, I. M. Large-scale analysis of CRISPR/Cas9 cell-cycle knockouts reveals the diversity of p53-dependent responses to cell-cycle defects. *Dev. Cell* **40**, 405–420.e402 (2017).
47. Petsalaki, E. & Zachos, G. An ATM-Chk2-INCENP pathway activates the abscission checkpoint. *J. Cell Biol.* **220**, e202008029 (2021).
48. Bakhoun, S. F., Kabeche, L., Murnane, J. P., Zaki, B. I. & Compton, D. A. DNA-damage response during mitosis induces whole-chromosome missegregation. *Cancer Discov.* **4**, 1281–1289 (2014).
49. Nai, S. et al. Chk2-dependent phosphorylation of myosin phosphatase targeting subunit 1 (MYPT1) regulates centrosome maturation. *Cell Cycle* **18**, 2651–2659 (2019).
50. von Schubert, C. et al. Plk1 and Mps1 cooperatively regulate the spindle assembly checkpoint in human cells. *Cell Rep.* **12**, 66–78 (2015).
51. Steegmaier, M. et al. BI 2536, a potent and selective inhibitor of polo-like kinase 1, inhibits tumor growth in vivo. *Curr. Biol.* **17**, 316–322 (2007).
52. Arienti, K. L. et al. Checkpoint kinase inhibitors: SAR and radio-protective properties of a series of 2-arylbenzimidazoles. *J. Med. Chem.* **48**, 1873–1885 (2005).

53. Cucchi, U. et al. Phosphorylation of TCTP as a marker for polo-like kinase-1 activity in vivo. *Anticancer Res.* **30**, 4973–4985 (2010).
54. DeBonis, S. et al. In vitro screening for inhibitors of the human mitotic kinesin Eg5 with antimitotic and antitumor activities. *Mol. Cancer Ther.* **3**, 1079–1090 (2004).
55. Rogakou, E. P., Pilch, D. R., Orr, A. H., Ivanova, V. S. & Bonner, W. M. DNA double-stranded breaks induce histone H2AX phosphorylation on serine 139. *J. Biol. Chem.* **273**, 5858–5868 (1998).
56. Hirao, A. et al. DNA damage-induced activation of p53 by the checkpoint kinase Chk2. *Science* **287**, 1824–1827 (2000).
57. Zegzouti, H., Zdanovskaia, M., Hsiao, K. & Goueli, S. A. ADP-Glo: a bioluminescent and homogeneous ADP monitoring assay for kinases. *Assay. Drug Dev. Technol.* **7**, 560–572 (2009).
58. Sharma, V. & Tepe, J. J. Potent inhibition of checkpoint kinase activity by a hymenialdisine-derived indolozepine. *Bioorg. Med. Chem. Lett.* **14**, 4319–4321 (2004).
59. Matsuoka, S. et al. Ataxia telangiectasia-mutated phosphorylates Chk2 in vivo and in vitro. *Proc. Natl Acad. Sci. USA* **97**, 10389–10394 (2000).
60. Schwarz, J. K., Lovly, C. M. & Piwnicka-Worms, H. Regulation of the Chk2 protein kinase by oligomerization-mediated cis- and trans-phosphorylation. *Mol. Cancer Res.* **1**, 598–609 (2003).
61. Kurz, E. U., Douglas, P. & Lees-Miller, S. P. Doxorubicin activates ATM-dependent phosphorylation of multiple downstream targets in part through the generation of reactive oxygen species. *J. Biol. Chem.* **279**, 53272–53281 (2004).
62. Hickson, I. et al. Identification and characterization of a novel and specific inhibitor of the ataxia-telangiectasia mutated kinase ATM. *Cancer Res.* **64**, 9152–9159 (2004).
63. Li, J. & Stern, D. F. Regulation of CHK2 by DNA-dependent protein kinase. *J. Biol. Chem.* **280**, 12041–12050 (2005).
64. Wang, X. Q., Redpath, J. L., Fan, S. T. & Stanbridge, E. J. ATR dependent activation of Chk2. *J. Cell Physiol.* **208**, 613–619 (2006).
65. Zenke, F. T. et al. Pharmacologic Inhibitor of DNA-PK, M3814, Potentiates Radiotherapy and Regresses Human Tumors in Mouse Models. *Mol. Cancer Ther.* **19**, 1091–1101 (2020).
66. Foote, K. M. et al. Discovery of 4-{4-[(3R)-3-Methylmorpholin-4-yl]-6-[1-(methylsulfonyl)cyclopropyl]pyrimidin-2-yl}-1H-indole (AZ20): a potent and selective inhibitor of ATR protein kinase with monotherapy in vivo antitumor activity. *J. Med. Chem.* **56**, 2125–2138 (2013).
67. Antonysamy, S. et al. Fragment-based discovery of JAK-2 inhibitors. *Bioorg. Med. Chem. Lett.* **19**, 279–282 (2009).
68. Lee, K. S., Grenfell, T. Z., Yarm, F. R. & Erikson, R. L. Mutation of the polo-box disrupts localization and mitotic functions of the mammalian polo kinase Plk. *Proc. Natl Acad. Sci. USA* **95**, 9301–9306 (1998).
69. Singh, P. et al. BUB1 and CENP-U, Primed by CDK1, Are the Main PLK1 Kinetochore Receptors in Mitosis. *Mol. Cell* **81**, 67–87.e69 (2021).
70. Vassilev, L. T. et al. Selective small-molecule inhibitor reveals critical mitotic functions of human CDK1. *Proc. Natl Acad. Sci. USA* **103**, 10660–10665 (2006).
71. Jiang, W. et al. PRC1: a human mitotic spindle-associated CDK substrate protein required for cytokinesis. *Mol. Cell* **2**, 877–885 (1998).
72. Gorgun, G. et al. A novel Aurora-A kinase inhibitor MLN8237 induces cytotoxicity and cell-cycle arrest in multiple myeloma. *Blood* **115**, 5202–5213 (2010).
73. Lasek, A. L., McPherson, B. M., Trueman, N. G. & Burkard, M. E. The functional significance of posttranslational modifications on polo-like kinase 1 revealed by chemical genetic complementation. *PLoS ONE* **11**, e0150225 (2016).
74. Hamanaka, R. et al. Polo-like kinase is a cell cycle-regulated kinase activated during mitosis. *J. Biol. Chem.* **270**, 21086–21091 (1995).
75. Lee, K. S. & Erikson, R. L. Plk is a functional homolog of *Saccharomyces cerevisiae* Cdc5, and elevated Plk activity induces multiple septation structures. *Mol. Cell Biol.* **17**, 3408–3417 (1997).
76. Mundt, K. E., Golsteyn, R. M., Lane, H. A. & Nigg, E. A. On the regulation and function of human polo-like kinase 1 (PLK1): effects of overexpression on cell cycle progression. *Biochem. Biophys. Res. Commun.* **239**, 377–385 (1997).
77. Nagy, Z., Comer, S. & Smolenski, A. Analysis of protein phosphorylation using phos-tag gels. *Curr. Protoc. Protein Sci.* **93**, e64 (2018).
78. Johnson, J. L. et al. An atlas of substrate specificities for the human serine/threonine kinome. *Nature* **613**, 759–766 (2023).
79. Seo, G. J. et al. Determination of substrate specificity and putative substrates of Chk2 kinase. *Biochem. Biophys. Res. Commun.* **304**, 339–343 (2003).
80. Moen, J. M. et al. Enhanced access to the human phosphoproteome with genetically encoded phosphothreonine. *Nat. Commun.* **13**, 7226 (2022).
81. Akopyan, K. et al. Assessing kinetics from fixed cells reveals activation of the mitotic entry network at the S/G2 transition. *Mol. Cell* **53**, 843–853 (2014).
82. Chouinard, G., Clement, I., Lafontaine, J., Rodier, F. & Schmitt, E. Cell cycle-dependent localization of CHK2 at centrosomes during mitosis. *Cell Div.* **8**, 7 (2013).
83. Li, X. H. et al. CHK2 is essential for spindle assembly and DNA repair during the first cleavage of mouse embryos. *Aging (Albany NY)* **12**, 10415–10426 (2020).
84. Kuniyasu, K., Iemura, K. & Tanaka, K. Delayed chromosome alignment to the spindle equator increases the rate of chromosome missegregation in cancer cell lines. *Biomolecules* **9** (2018).
85. Agustinus, A. S. et al. Epigenetic dysregulation from chromosomal transit in micronuclei. *Nature* **619**, 176–183 (2023).
86. Papathanasiou, S. et al. Heritable transcriptional defects from aberrations of nuclear architecture. *Nature* **619**, 184–192 (2023).
87. Joo, Y. K. et al. ATR promotes clearance of damaged DNA and damaged cells by rupturing micronuclei. *Mol. Cell* **83**, 3642–3658.e3644 (2023).
88. Zhang, C. Z. et al. Chromothripsis from DNA damage in micronuclei. *Nature* **522**, 179–184 (2015).
89. Hatch, E. M., Fischer, A. H., Deerinck, T. J. & Hetzer, M. W. Catastrophic nuclear envelope collapse in cancer cell micronuclei. *Cell* **154**, 47–60 (2013).
90. Wood, K. W. et al. Antitumor activity of an allosteric inhibitor of centromere-associated protein-E. *Proc. Natl Acad. Sci. USA* **107**, 5839–5844 (2010).
91. Santaguida, S., Tighe, A., D’Alise, A. M., Taylor, S. S. & Musacchio, A. Dissecting the role of MPS1 in chromosome biorientation and the spindle checkpoint through the small molecule inhibitor reversine. *J. Cell Biol.* **190**, 73–87 (2010).
92. Degenhardt, Y. & Lampkin, T. Targeting Polo-like kinase in cancer therapy. *Clin. Cancer Res.* **16**, 384–389 (2010).
93. Colaco, V. et al. In silico and structure-based evaluation of deleterious mutations identified in human Chk1, Chk2, and Wee1 protein kinase. *J. Cell Biochem.* **125**, 88–89 (2023).
94. Niida, H. et al. Cooperative functions of Chk1 and Chk2 reduce tumour susceptibility in vivo. *EMBO J.* **29**, 3558–3570 (2010).
95. Fujiwara, T. et al. Cytokinesis failure generating tetraploids promotes tumorigenesis in p53-null cells. *Nature* **437**, 1043–1047 (2005).
96. Crasta, K. et al. DNA breaks and chromosome pulverization from errors in mitosis. *Nature* **482**, 53–58 (2012).
97. Apostolou, P. & Papatirou, I. Current perspectives on CHEK2 mutations in breast cancer. *Breast Cancer (Dove Med Press)* **9**, 331–335 (2017).
98. Cybulski, C. et al. CHEK2 is a multiorgan cancer susceptibility gene. *Am. J. Hum. Genet.* **75**, 1131–1135 (2004).

99. Cybulski, C. et al. A novel founder CHEK2 mutation is associated with increased prostate cancer risk. *Cancer Res.* **64**, 2677–2679 (2004).
100. Kabeche, L., Nguyen, H. D., Buisson, R. & Zou, L. A mitosis-specific and R loop-driven ATR pathway promotes faithful chromosome segregation. *Science* **359**, 108–114 (2018).
101. Zachos, G. et al. Chk1 is required for spindle checkpoint function. *Dev. Cell* **12**, 247–260 (2007).
102. Bruinsma, W. et al. Spatial separation of Plk1 phosphorylation and activity. *Front. Oncol.* **5**, 132 (2015).
103. Lindqvist, A., Rodriguez-Bravo, V. & Medema, R. H. The decision to enter mitosis: feedback and redundancy in the mitotic entry network. *J. Cell Biol.* **185**, 193–202 (2009).
104. van Vugt, M. A. et al. A mitotic phosphorylation feedback network connects Cdk1, Plk1, 53BP1, and Chk2 to inactivate the G(2)/M DNA damage checkpoint. *PLoS Biol.* **8**, e1000287 (2010).
105. Bakhoum, S. F., Genovese, G. & Compton, D. A. Deviant kinetochore microtubule dynamics underlie chromosomal instability. *Curr. Biol.* **19**, 1937–1942 (2009).
106. Bakhoum, S. F., Thompson, S. L., Manning, A. L. & Compton, D. A. Genome stability is ensured by temporal control of kinetochore-microtubule dynamics. *Nat. Cell Biol.* **11**, 27–35 (2009).
107. Manning, A. L. et al. CLASP1, astrin and Kif2b form a molecular switch that regulates kinetochore-microtubule dynamics to promote mitotic progression and fidelity. *EMBO J.* **29**, 3531–3543 (2010).
108. Liu, D., Vader, G., Vromans, M. J., Lampson, M. A. & Lens, S. M. Sensing chromosome bi-orientation by spatial separation of aurora B kinase from kinetochore substrates. *Science* **323**, 1350–1353 (2009).
109. Roshan X. Norman, R. F. L., Anuoluwapo A. Mattix, Zhouyuan Shen, Caleb L. Carlsen, Mark E. Burkard. Dynamic Plk1 recruitment to the inner centromere. *BioRxiv* <https://doi.org/10.1101/2024.07.03.601947> (2024).
110. Peterson, A. C., Russell, J. D., Bailey, D. J., Westphall, M. S. & Coon, J. J. Parallel reaction monitoring for high resolution and high mass accuracy quantitative, targeted proteomics. *Mol. Cell Proteom.* **11**, 1475–1488 (2012).
111. MacLean, B. et al. Skyline: an open source document editor for creating and analyzing targeted proteomics experiments. *Bioinformatics* **26**, 966–968 (2010).
112. Shevchenko, A., Tomas, H., Havlis, J., Olsen, J. V. & Mann, M. In-gel digestion for mass spectrometric characterization of proteins and proteomes. *Nat. Protoc.* **1**, 2856–2860 (2006).
113. Suzuki, Y. et al. FGF23 contains two distinct high-affinity binding sites enabling bivalent interactions with alpha-Klotho. *Proc. Natl Acad. Sci. USA* **117**, 31800–31807 (2020).

Acknowledgements

This work is supported by the Pershing Square Sohn Cancer Alliance Award (LK), R35 GM150648-01 (LK), R01GM137031 (YL), 1F31CA275096-01A1 (EB),

and Gruber Science Fellowship (EB). We thank Dr. Mark Burkard for generously providing RPE-1 asPLK1 cells, Dr. Jesse Reinhart for providing the wild-type and kinase-dead Chk2 protein, Dr. Claudio Alarcon for pGEX6p-1 plasmid, and Drs. Michael Yaffe, Kevin Janes, Michael Lampson, and Bob Weinberg for reagents. We thank Denis Ostapenko for critical feedback on the manuscript.

Author contributions

E.B. and L.K. designed the study. E.B., I.T., C.R., Y.K.J., J.P., W.L., and Y.L., performed the experiments and analyses. E.B. and L.K. prepared the paper with contributions from all authors.

Competing interests

The authors declare no competing interests.

Additional information

Supplementary information The online version contains supplementary material available at <https://doi.org/10.1038/s41467-024-54922-7>.

Correspondence and requests for materials should be addressed to Lilian Kabeche.

Peer review information *Nature Communications* thanks the anonymous reviewers for their contribution to the peer review of this work. A peer review file is available.

Reprints and permissions information is available at <http://www.nature.com/reprints>

Publisher's note Springer Nature remains neutral with regard to jurisdictional claims in published maps and institutional affiliations.

Open Access This article is licensed under a Creative Commons Attribution-NonCommercial-NoDerivatives 4.0 International License, which permits any non-commercial use, sharing, distribution and reproduction in any medium or format, as long as you give appropriate credit to the original author(s) and the source, provide a link to the Creative Commons licence, and indicate if you modified the licensed material. You do not have permission under this licence to share adapted material derived from this article or parts of it. The images or other third party material in this article are included in the article's Creative Commons licence, unless indicated otherwise in a credit line to the material. If material is not included in the article's Creative Commons licence and your intended use is not permitted by statutory regulation or exceeds the permitted use, you will need to obtain permission directly from the copyright holder. To view a copy of this licence, visit <http://creativecommons.org/licenses/by-nc-nd/4.0/>.

© The Author(s) 2024